

# Generalized Low-Rank Matrix Completion Model with Overlapping Group Error Representation

Wenjing Lu, Zhuang Fang, Liang Wu, Liming Tang, and Hanxin Liu

**Abstract**—The low-rank matrix completion (LRMC) technology has achieved remarkable results in low-level visual tasks. There is an underlying assumption that the real-world matrix data is low-rank in LRMC. However, the real matrix data does not satisfy the strict low-rank property, which undoubtedly present serious challenges for the above-mentioned matrix recovery methods. Fortunately, there are feasible schemes that devise appropriate and effective priori representations for describing the intrinsic information of real data. In this paper, we firstly model the matrix data  $\mathbf{Y}$  as the sum of a low-rank approximation component  $\mathbf{X}$  and an approximation error component  $\mathcal{E}$ . This finer-grained data decomposition architecture enables each component of information to be portrayed more precisely. Further, we design an overlapping group error representation (OGER) function to characterize the above error structure and propose a generalized low-rank matrix completion model based on OGER. Specifically, the low-rank component describes the global structure information of matrix data, while the OGER component not only compensates for the approximation error between the low-rank component and the real data but also better captures the local block sparsity information of matrix data. Finally, we develop an alternating direction method of multipliers (ADMM) that integrates the majorization-minimization (MM) algorithm, which enables the efficient solution of the proposed model. And we analyze the convergence of the algorithm in detail both theoretically and experimentally. In addition, the results of numerical experiments demonstrate that the proposed model outperforms existing competing models in performance.

**Index Terms**—Low-rank, matrix completion, approximation error, overlapping group, block sparsity.

## I. INTRODUCTION

**L**OW-RANK matrix completion has been extensively used in various fields as an essential technical tool for handling incomplete observation matrices, including recommender systems [1]–[3], image restoration [4]–[6], motion capture [7]–[9], and background subtraction [10]–[12], etc. In practical applications, real matrix data is frequently corrupted due to unavoidable reasons, such as missing data, noise pollution, and text overwriting. In recent years, numerous methods have emerged that utilize low-rank priors to recover unknown

low-rank matrices. The low-rank matrix completion can be expressed as the following minimization problem,

$$\begin{aligned} \min_{\mathbf{X}} \quad & \text{rank}(\mathbf{X}) \\ \text{s.t.} \quad & \mathbf{Y}_\Omega = \mathbf{X}_\Omega, \end{aligned} \quad (1)$$

where  $\Omega$  is the set of positional indices of observable matrix data  $\mathbf{Y}_\Omega$ ,  $\mathbf{X}$  is the original matrix data. However, the rank minimization problem is NP-hard due to the discontinuity and non-convexity of the rank function. Therefore, finding a suitable approximation of the rank function is crucial in solving above problem [13]–[15]. To achieve the most accurate approximation of rank functions, nuclear norm minimization (NNM) model [16], [17] have been proposed, which exploit the property of the nuclear norm as the tightest convex relaxation of the rank function and recover incomplete matrices from observation matrices containing only partial entries. The standard nuclear norm is defined as the sum of the singular values of matrix  $\mathbf{X}$ , denoted as  $\|\mathbf{X}\|_* = \sum_i \|\sigma_i(\mathbf{X})\|_1$ , where  $\sigma_i(\mathbf{X})$  represents the  $i$ -th singular value of matrix  $\mathbf{X}$ . However, the standard nuclear norm shrinks equally for each singular value, which results in only suboptimal performance in practical recovery applications.

Recently, several scholars have attempted to approximate the rank function utilizing non-convex functions in order to improve the data recovery performance [18]–[24]. In particular, Gu et al. in [20] and [21] considered the disparity among different singular values and introduced the weighted nuclear norm minimization (WNNM) model, which optimizes the recovery effect through adaptive weighting. Inspired by the WNNM model, the weighted Schatten  $p$ -norm was proposed in [25], serving as a low-rank matrix approximation method capable of capturing subtle features in matrix structures. Furthermore, Li et al. [22] ingeniously combined the advantages of the Schatten  $p$ -norm and the capped norm, devising the Schatten capped  $p$  (SCP) norm, which achieves a balance between the rank and nuclear norm of the matrix. Subsequently, the introduction of an adaptive weight function strategy [26] in low-rank matrix/tensor complementation provides a more flexible method for adaptively assigning singular value weights. Gao et al. [27] proposed a novel non-convex surrogate of the rank function, utilizing the ratio of the nuclear norm to the Frobenius norm. These models based on non-convex surrogate functions have achieved remarkable recovery effects in practical applications, owing to their ability to accurately portray the complex properties of matrix data.

Although the above models have indeed improved the performance of data restoration to some extent, there remains a

W. Lu (first author) is with the School of Mathematics and Statistics, Hubei Minzu University, Enshi 44500, Hubei, China (email: luwenjing07@163.com).

Z. Fang (corresponding author) is with the School of Mathematics and Statistics, Hubei Minzu University, Enshi 44500, Hubei, China. (email: wdfangzhuang@163.com).

L. Wu is with the School of Mathematics and Statistics, Southwest University, Chongqing, 400715, China (email: liangwu1998@163.com).

L. Tang and H. Liu are with the School of Mathematics and Statistics, Hubei Minzu University, Enshi 44500, Hubei, China (email: tlmc87@foxmail.com, 2531417503@qq.com).

pressing issue that demands further exploration. That is, these models often assume that the matrix data possesses strict low-rank properties and relies solely on low-rank representations to characterize the essential features of the data in modeling [28], [29]. At present, robust principal component analysis (RPCA) [30], [31], is a widely adopted decomposition method, which decomposes the real matrix data  $\mathbf{Y}$  into a low-rank component  $\mathbf{X}$  and a sparse component  $\mathbf{S}$ . It models the decomposition as follows,

$$\begin{aligned} \min_{\mathbf{X}} \quad & \text{rank}(\mathbf{X}) + \lambda \|\mathbf{S}\|_0 \\ \text{s.t.} \quad & \mathbf{Y} = \mathbf{X} + \mathbf{S}, \end{aligned} \quad (2)$$

where  $\mathbf{S}$  is employed to capture noise, outliers, or corrupted portions of the matrix data, and  $\lambda$  is a positive regularization parameter. Similar to problem (1), problem (2) is also an NP-hard problem due to the non-convexity of the rank function and the  $L^0$ -norm. To facilitate handling this problem, the nuclear norm and  $L^1$ -norm were introduced in [32] as convex approximations to the rank function and  $L^0$ -norm in problem (2), respectively.

Recent studies have shown that non-convex functions often exhibit superior performance over convex functions in addressing the optimization problem of rank function relaxation. For instance, a novel non-convex penalty sparse component method was developed in [33], which achieves effective minimization via generalized shrinkage. The application of non-convex total variation regularization to sparse matrices in [34] enhances matrix sparsity in the gradient domain, thereby improving solution accuracy. To further preserve more information within matrix data, a new non-convex sparse function was constructed in [35] to replace traditional sparsity constraints. Considering the effectiveness of minimally-concave penalty (MCP) as a sparsity-inducing regularization, Pokala et al. [36] proposed a method that can accurately achieve low-rank sparse matrix factorization. Especially, a solvable algorithm targeting the  $L^0$  norm is proposed [37], albeit at the cost of increased computational complexity. It is worth noting that the non-convex relaxation method mentioned above mainly focuses on point sparse modeling, which may fall short of capturing more complex structural features present in matrix data.

However, there are two main shortcomings of the above methods. On the one hand, most of the methods mentioned above inherently assume that the sparse components decomposed from modeling are solely noise, overlooking the sparse detail information intrinsic to original data. On the other hand, these methods do not focus on the description of sparse data for structural blocks. Therefore, there is a large approximation error between the reconstructed low-rank matrix data and the original matrix data. In fact, the real data is not merely comprised of low-rank matrix, but is composed of both low-rank component and structured sparse component, as shown in Fig. 1. Thus, it is a critical challenge to design an appropriate and accurate prior representation function for capturing structured sparse detail elements of real data.

#### A. Our Contributions

In this paper, we propose a generalized low-rank matrix completion model with overlapping group error representation

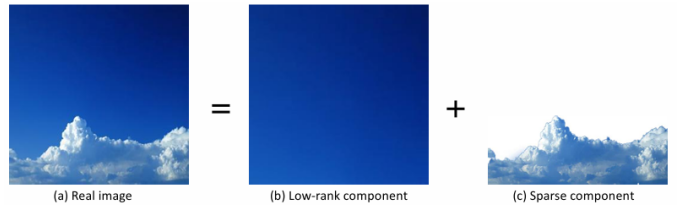


Fig. 1: An example of the decomposition result of a real image.

(OGER). And the contributions of this paper are concluded as follows:

1) First, we design a priori operator for inscribing the matrix with structured sparse properties, which is called the OGER function in this paper (see Definition 8). On this basis, a novel decomposition framework of the real low-rank matrix data  $\mathbf{Y}$  is proposed as

$$\mathbf{Y} = \mathbf{X} + \mathcal{E},$$

where  $\mathbf{X}$  and  $\mathcal{E}$  are the low-rank component and the structured sparse component, respectively. This novel form of data decomposition effectively decomposes a complex data matrix into two components with distinct characteristics, which provides accurate modeling for further operations.

2) Second, based on the above decomposition framework, we propose a mathematical model for low-rank matrix completion (more detailed technical steps please see Fig. 2), which is described as

$$\begin{aligned} \min_{\mathbf{X}, \mathcal{E}} \quad & R(\mathbf{X}) + \lambda \phi(\mathcal{E}) \\ \text{s.t.} \quad & \mathbf{Y}_\Omega = \mathbf{X}_\Omega + \mathcal{E}_\Omega, \end{aligned}$$

where  $\lambda > 0$  is a regularization parameter,  $\Omega$  is the set of positional indices of observable matrix data  $\mathbf{Y}_\Omega$ ,  $\mathbf{X}$  and  $\mathcal{E}$  are the low-rank component and structured sparse component, respectively. By minimizing the above model, it is possible to efficiently obtain the low-rank part  $\mathbf{X}$  and the structured sparse part  $\mathcal{E}$  from the observed matrix  $\mathbf{Y}_\Omega$  with missing values. Further, the recovered data  $\mathbf{Y}^*$  is mathematically represented as the sum of these two matrix components, i.e.,  $\mathbf{Y}^* = \mathbf{X} + \mathcal{E}$ .

3) Third, we propose an efficient alternating direction method of multipliers (ADMM) [38]–[40] that integrates the majorization-minimization (MM) algorithm [36], [41], [42] to solve the above proposed model. We analyze the proposed model and algorithm, and notice that they perform better mathematical properties including convexity of OGER (Section III-A), convergence of the algorithm (Section IV-E) and so on. In addition, numerous numerical experimental results show that the proposed model and algorithm achieve excellent performance in matrix completion. Compared with other state-of-the-art models, our method still has a large advantage.

#### B. Organization

The remainder of this paper is structured as follows. Section II presents definitions and theorems pertinent to low-rank matrix completion methods. Section III provides a detailed exposition of the proposed model and its corresponding solution algorithm. The numerical experimental results of the model and a discussion of its parameters are shown in Section IV. Finally, Section V summarizes the entire manuscript.

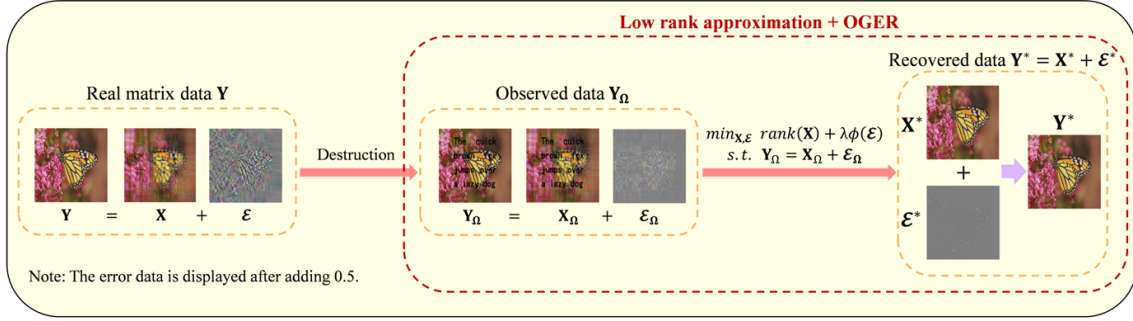


Fig. 2: Illustration of the proposed method.

## II. PRELIMINARIES AND PROBLEM FORMULATION

The low-rank matrix completion methods have been extensively studied owing to their widespread applications in computer vision and machine learning [43], [44]. In this section, we mainly review some definitions and theorems related to low-rank matrix completion methods.

**Definition 1** (SVD [45]). For any given matrix  $\mathbf{M} \in \mathbb{R}^{n_1 \times n_2}$ , its singular value decomposition is  $\mathbf{M} = \mathbf{U}_\mathbf{M} \Sigma_\mathbf{M} \mathbf{V}_\mathbf{M}^T$ , where  $\mathbf{U}_\mathbf{M} \in \mathbb{R}^{n_1 \times n_1}$ ,  $\mathbf{V}_\mathbf{M} \in \mathbb{R}^{n_2 \times n_2}$  are both orthogonal matrices,  $\Sigma_\mathbf{M} \in \mathbb{R}^{n_1 \times n_2}$  is a diagonal matrix, and the elements  $\sigma_1 \dots \sigma_r$  on its diagonal are the singular values of  $\mathbf{M}$  and

$$\Sigma_\mathbf{M} = \begin{bmatrix} \sigma_1 & & & \\ & \ddots & & \\ & & \sigma_r & \\ & & & \end{bmatrix}.$$

**Definition 2** (Rank Function [45]). For a given matrix  $\mathbf{M} \in \mathbb{R}^{n_1 \times n_2}$  satisfying the SVD, if  $r = \min\{n_1, n_2\}$  and the singular values of matrix  $\mathbf{M}$  are  $\sigma_1 \geq \sigma_2 \geq \sigma_3 \geq \dots \geq \sigma_r$ , then the rank function of matrix  $\mathbf{M}$  can be defined as the number of nonzero singular values in  $\mathbf{M}$  can be expressed as follows,

$$\text{rank}(\mathbf{M}) = \|\Sigma_\mathbf{M}\|_0 = \#\{i | \sigma_i(\mathbf{M}) \neq 0\}.$$

**Definition 3** (Nuclear Norm [16], [17]). For a given matrix  $\mathbf{M} \in \mathbb{R}^{n_1 \times n_2}$  satisfying the SVD, if  $r = \min\{n_1, n_2\}$  and the singular values of matrix  $\mathbf{M}$  are  $\sigma_1 \geq \sigma_2 \geq \sigma_3 \geq \dots \geq \sigma_r$ , then the nuclear norm of matrix  $\mathbf{M}$  can be expressed as the following form,

$$\|\mathbf{M}\|_* = \sum_{i=1}^{\min\{n_1, n_2\}} \sigma_i(\mathbf{M}).$$

**Definition 4** (Schatten  $p$  Norm [19]). For a given matrix  $\mathbf{M} \in \mathbb{R}^{n_1 \times n_2}$  satisfying the SVD, if  $r = \min\{n_1, n_2\}$  and the singular values of matrix  $\mathbf{M}$  are  $\sigma_1 \geq \sigma_2 \geq \sigma_3 \geq \dots \geq \sigma_r$ , then the Schatten  $p$  norm of matrix  $\mathbf{M}$  can be expressed as the following form,

$$\|\mathbf{M}\|_{S_p} = \left( \sum_{i=1}^{\min\{n_1, n_2\}} \sigma_i(\mathbf{M})^p \right)^{1/p},$$

where  $0 < p \leq 1$  is a scale parameter.

**Definition 5** (Weighted Nuclear Norm [20], [21]). For a given matrix  $\mathbf{M} \in \mathbb{R}^{n_1 \times n_2}$  satisfying the SVD, if  $r = \min\{n_1, n_2\}$  and the singular values of matrix  $\mathbf{M}$  are  $\sigma_1 \geq \sigma_2 \geq \sigma_3 \geq \dots \geq \sigma_r$ , then the weighted nuclear norm of matrix  $\mathbf{M}$  can be expressed as the following form,

$\dots \geq \sigma_r$ , then the weighted nuclear norm of matrix  $\mathbf{M}$  can be expressed as the following form,

$$\|\mathbf{M}\|_{\mathbf{w},*} = \sum_{i=1}^{\min\{n_1, n_2\}} \|w_i \sigma_i(\mathbf{M})\|_1,$$

where  $w_i \geq 0$  are weight coefficients.

**Definition 6** (Weighted Schatten  $p$  Norm [25]). For a given matrix  $\mathbf{M} \in \mathbb{R}^{n_1 \times n_2}$  satisfying the SVD, if  $r = \min\{n_1, n_2\}$  and the singular values of matrix  $\mathbf{M}$  are  $\sigma_1 \geq \sigma_2 \geq \sigma_3 \geq \dots \geq \sigma_r$ , then the weighted Schatten  $p$  norm of matrix  $\mathbf{M}$  can be expressed as the following form,

$$\|\mathbf{M}\|_{\mathbf{w},S_p} = \left( \sum_{i=1}^{\min\{n_1, n_2\}} w_i \sigma_i(\mathbf{M})^p \right)^{1/p},$$

where  $w_i \geq 0$  and  $0 < p \leq 1$  are weight coefficients and scale parameter, respectively.

**Definition 7** (Schatten Capped  $p$  Norm [22]). For a given matrix  $\mathbf{M} \in \mathbb{R}^{n_1 \times n_2}$  satisfying the SVD, if  $r = \min\{n_1, n_2\}$  and the singular values of matrix  $\mathbf{M}$  are  $\sigma_1 \geq \sigma_2 \geq \sigma_3 \geq \dots \geq \sigma_r$ , then the Schatten capped  $p$  norm of matrix  $\mathbf{M}$  can be expressed as the following form,

$$\|\mathbf{M}\|_{S_{p,\tau}} = \left( \sum_{i=1}^{\min\{n_1, n_2\}} \min(\sigma_i(\mathbf{M}), \tau)^p \right)^{1/p},$$

where  $\tau \geq 0$  and  $0 < p \leq 1$  are shrinkage threshold and scale parameter, respectively.

**Theorem 1** (MM Algorithm [36], [41], [42]). If  $f(u)$  is a smooth function, consider the optimization problem,

$$u^* = \underset{u}{\operatorname{argmin}} f(u)$$

the solution of the following iterative optimization problem converges to the solution  $u^*$  of the above minimization problem as  $n \rightarrow \infty$ ,

$$u_{n+1} = \underset{u}{\operatorname{argmin}} g(u, u_n),$$

where the surrogate function  $g(u, u_n)$  satisfies: (i) For any  $u$ ,  $g(u_n, u_n) = f(u_n)$  and (ii)  $g(u, u_n) \geq f(u)$ . The detailed optimization steps are shown in Algorithm 1.

**Remark 1.** When the original objective function in an optimization problem has a complex structure, we usually seek an surrogate function that satisfies the above two preconditions to facilitate the simplification of the form of the function. In

**Algorithm 1** MM algorithm

---

**Input:**  $g(\cdot)$ ,  $N$ .  
1: Initialize  $u$  and  $n = 0$ .  
2: **while** not converged **do**  
3:   Update  $u_{n+1}$  by  $u_{n+1} = \arg \min_u g(u, u_n)$ ;  
4:    $n = n + 1$ .  
5: **end while**  
**Output:**  $u^* = u_{n+1}$ .

---

general, the surrogate function is convex in nature. In this case, it is pointed out in the literature [46] that if the original objective function  $f(u)$  is convex, as  $n \rightarrow \infty$ , the solution  $u_{n+1}$  obtained by the MM algorithm converges to the original actual minimum point  $u^*$ ; if the original objective function  $f(u)$  is nonconvex, as  $n \rightarrow \infty$ , the solution  $u_{n+1}$  obtained by the MM algorithm converges to the extreme value point (also called the stabilization point) of the original objective function.

### III. ESTABLISHMENT OF THE MODEL

As mentioned in the introduction section, most real data are not strictly low-rank, and thus it is not accurate to portray their essential features solely through low-rank representations. In this section, we first analyze the degree of discrepancy between the recovered data and the real data under the strict low-rank assumption, based on the rank-approximation error representation (see Theorem 2). Secondly, we deeply analyze the structural features of the error data, design a prior function to characterize the approximation error, and a new decomposition architecture (low-rank and overlapping group error representation) for real data is proposed. Finally, based on this new matrix data decomposition framework, a class of generalized low-rank matrix complementary models and corresponding solution algorithms are proposed.

#### A. Overlapping Group Error Representation

**Theorem 2** ( $k$ -rank Approximation Error [47]). *For a given matrix  $\mathbf{M} \in \mathbb{R}^{n_1 \times n_2}$  satisfying the SVD,  $\mathbf{M}_k$  is the best approximation matrix of rank  $k$  of  $\mathbf{M}$ . Then  $\|\mathbf{M} - \mathbf{M}_k\|_F^2$  can be represented by the singular values  $\sigma_i$  of  $\mathbf{M}$ .*

The proof of Theorem 2 is provided in Appendix A.

Theorem 2 describes the error transformations relation between a matrix and its best approximation matrix of rank  $k$ . It is evident that as  $k$  decreases, the rank approximation error increases. There is a contradiction between the lower rank approximation representation and the rank approximation error. Specifically, a lower-rank approximation benefits LRMC but leads to a larger approximation error. We find that the root cause of this phenomenon is that the matrix data is not strictly low-rank and the approximation error is not negligible. Consequently, characterizing the matrix solely based on its low rank is unreasonable.

To better measure the inherent information of data, we propose a novel decomposition framework for real data. The decomposition model is as follows,

$$\mathbf{Y} = \mathbf{X} + \mathcal{E}, \quad (3)$$

where  $\mathbf{Y}$  is the real matrix,  $\mathbf{X}$  and  $\mathcal{E}$  are the low-rank component and error component, respectively. The decomposition model divides the matrix data into a low-rank component and an error component, thereby enabling a more accurate measurement of the sparse properties inherent in the data.

Therefore, to find a suitable priori function to describe the above error components, we have conducted some decomposition experiments. We selected two test images ‘Babala’ and ‘Butterfly’ and set the settings to different levels such as 100, 70, 50, 40, 30, 20, and 10. The corresponding low-rank and sparse components after interception are shown in Fig. 3. Among them, the first and third rows are the low-rank components and the second and fourth rows are the sparse components. It can be observed from Fig. 3 that as the  $k$  value decreases, the approximation image tends to retain only information such as texture and details, making the overall effect of the image more blurred; Meanwhile, the error image tends to retain only information such as edges and contours, giving the image a more structured overall effect.

To address the significant structural block sparsity property of the error matrix data in the case of a smaller  $k$ -value approximation, we design an overlapping group error representation (OGER) function to effectively characterize the structural block sparsity of the matrix.

**Definition 8** (OGER Function). *For any matrix  $\mathcal{E} \in \mathbb{R}^{n_1 \times n_2}$ , its OGER function  $\phi(\mathcal{E})$  is defined as*

$$\begin{aligned} \phi(\mathcal{E}) &= \sum_{i,j=1} \left[ \sum_{k_1, k_2=-n_1}^{n_2} |\varepsilon(i+k_1, j+k_2)|^2 \right]^{\frac{1}{2}} \\ &= \sum_{i,j=1} \|\mathcal{E}_{(i,j),K}\|_2, \end{aligned} \quad (4)$$

where,  $n_1 = \lfloor \frac{K-1}{2} \rfloor$ ,  $n_2 = \lfloor \frac{K}{2} \rfloor$ , and  $\mathcal{E}_{(i,j),K}$  is defined as a  $K * K$  point group at index set  $(i, j)$ ,

$$\mathcal{E}_{(i,j),K} = \begin{bmatrix} \varepsilon(i-n_1, j-n_1) & \varepsilon(i-n_1, j-n_1+1) & \cdots & \varepsilon(i-n_1, j+n_2) \\ \varepsilon(i-n_1+1, j-n_1) & \varepsilon(i-n_1+1, j-n_1+1) & \cdots & \varepsilon(i-n_1+1, j+n_2) \\ \vdots & \vdots & \ddots & \vdots \\ \varepsilon(i+n_2, j-n_1) & \varepsilon(i+n_2, j-n_1+1) & \cdots & \varepsilon(i+n_2, j+n_2) \end{bmatrix}.$$

**Theorem 3** (OGER Convexity). *For any matrix  $\mathcal{E} \in \mathbb{R}^{n_1 \times n_2}$ , its overlapping group function  $\phi(\mathcal{E})$  is a convex function.*

The proof of Theorem 3 is provided in Appendix B.

**Remark 2.** *OGER serves as an a priori function for inscribing matrices presenting sparse properties of structural blocks. Compared to the universal point-sparse ( $L^1$ -norm) representation, this inscription captures nonlocal sparse blocks in the error components more efficiently and describes the mathematical structure of such matrices more accurately. Furthermore, when  $K = 1$ , the OGER function reduces to a universal point-sparse representation.*



Fig. 3: Decomposition results of ‘Babala’ and ‘Butterfly’ test images for different low-rank truncations.

### B. The Proposed Model and Algorithm

In this subsection, we embed the OGER into the generalized low-rank matrix completion model and construct a novel generalized low-rank matrix completion model with overlapping group error representation. The proposed model utilizes the group sparsity metric to address the connection between pixel points in the local region, maintaining the local coherence and stability of the matrix, while effectively preserving the sparse texture and structure in the restored data to achieve superior restoration results. The specific model is as follows,

$$\begin{aligned} & \min_{\mathbf{X}, \mathcal{E}} R(\mathbf{X}) + \lambda \phi(\mathcal{E}) \\ & \text{s.t. } \mathbf{Y}_\Omega = \mathbf{X}_\Omega + \mathcal{E}_\Omega, \end{aligned} \quad (5)$$

where  $\lambda$  is a positive parameter,  $\mathbf{X}$  and  $\mathcal{E}$  are the low-rank component and structural error component, respectively. And  $\mathbf{Y}_\Omega$  is the observed matrix data,  $\Omega$  is the indexed set of uncorrupted points,  $R(\mathbf{X})$  is the approximation function of the rank function, and  $\phi(\mathcal{E})$  denotes the OGER function used to characterize the structural error. By the primal-dual theory [48], Eq. (5) can be rewritten as

$$\min_{\mathbf{X}, \mathcal{E}} \alpha R(\mathbf{X}) + \lambda \phi(\mathcal{E}) + \frac{1}{2} \|\mathbf{Y}_\Omega - \mathbf{X}_\Omega - \mathcal{E}_\Omega\|_F^2, \quad (6)$$

where  $\alpha$  and  $\lambda$  represent the regularization parameters.

The ADMM algorithm is used to solve the above problems. To begin with, we introduce auxiliary variables  $\mathbf{W}$ ,  $\mathbf{E}$ , and  $\mathbf{F}_\Omega$ . Then, we reformulate the above formula by rewriting it as the following,

$$\begin{aligned} & \min_{\mathbf{X}, \mathcal{E}, \mathbf{W}, \mathbf{E}, \mathbf{F}_\Omega} \alpha R(\mathbf{W}) + \lambda \phi(\mathbf{E}) + \frac{1}{2} \|\mathbf{F}_\Omega\|_F^2 \\ & \text{s.t. } \mathbf{W} = \mathbf{X}, \mathbf{E} = \mathcal{E}, \mathbf{F}_\Omega = \mathbf{Y}_\Omega - \mathbf{X}_\Omega - \mathcal{E}_\Omega. \end{aligned} \quad (7)$$

Therefore, the augmented Lagrangian function of the problem (7) can be written as

$$\begin{aligned} L(\mathbf{X}, \mathbf{W}, \mathcal{E}, \mathbf{F}_\Omega, \mathbf{E}, \boldsymbol{\mu}_1, \boldsymbol{\mu}_2, \boldsymbol{\mu}_3) = & \\ & \alpha R(\mathbf{W}) + \lambda \phi(\mathbf{E}) + \frac{1}{2} \|\mathbf{F}_\Omega\|_F^2 \\ & + \frac{\rho}{2} \left\| \mathbf{W} - \mathbf{X} + \frac{\boldsymbol{\mu}_1}{\rho} \right\|_F^2 + \frac{\rho}{2} \left\| \mathbf{E} - \mathcal{E} + \frac{\boldsymbol{\mu}_2}{\rho} \right\|_F^2 \\ & + \frac{\rho}{2} \left\| \mathbf{F}_\Omega - (\mathbf{Y}_\Omega - \mathbf{X}_\Omega - \mathcal{E}_\Omega) + \frac{\boldsymbol{\mu}_3}{\rho} \right\|_F^2, \end{aligned} \quad (8)$$

where,  $\boldsymbol{\mu}_1$ ,  $\boldsymbol{\mu}_2$  and  $\boldsymbol{\mu}_3$  are Lagrange multipliers, and  $\rho > 0$  is the penalty parameter. All subproblems are described as

$$\begin{cases} \mathbf{X}^{k+1} = \arg \min_{\mathbf{X}} L(\mathbf{X}, \mathbf{W}^k, \mathcal{E}^k, \mathbf{F}_\Omega^k, \mathbf{E}^k, \boldsymbol{\mu}_1^k, \boldsymbol{\mu}_2^k, \boldsymbol{\mu}_3^k) \\ \mathbf{W}^{k+1} = \arg \min_{\mathbf{W}} L(\mathbf{X}^{k+1}, \mathbf{W}, \mathcal{E}^k, \mathbf{F}_\Omega^k, \mathbf{E}^k, \boldsymbol{\mu}_1^k, \boldsymbol{\mu}_2^k, \boldsymbol{\mu}_3^k) \\ \mathcal{E}^{k+1} = \arg \min_{\mathcal{E}} L(\mathbf{X}^{k+1}, \mathbf{W}^{k+1}, \mathcal{E}, \mathbf{F}_\Omega^k, \mathbf{E}^k, \boldsymbol{\mu}_1^k, \boldsymbol{\mu}_2^k, \boldsymbol{\mu}_3^k) \\ \mathbf{F}_\Omega^{k+1} = \arg \min_{\mathbf{F}_\Omega} L(\mathbf{X}^{k+1}, \mathbf{W}^{k+1}, \mathcal{E}^{k+1}, \mathbf{F}_\Omega, \mathbf{E}^k, \boldsymbol{\mu}_1^k, \boldsymbol{\mu}_2^k, \boldsymbol{\mu}_3^k) \\ \mathbf{E}^{k+1} = \arg \min_{\mathbf{E}} L(\mathbf{X}^{k+1}, \mathbf{W}^{k+1}, \mathcal{E}^{k+1}, \mathbf{F}_\Omega^{k+1}, \mathbf{E}, \boldsymbol{\mu}_1^k, \boldsymbol{\mu}_2^k, \boldsymbol{\mu}_3^k) \\ \boldsymbol{\mu}_1^{k+1} = \boldsymbol{\mu}_1^k + \rho(\mathbf{W}^{k+1} - \mathbf{X}^{k+1}) \\ \boldsymbol{\mu}_2^{k+1} = \boldsymbol{\mu}_2^k + \rho(\mathbf{E}^{k+1} - \mathcal{E}^{k+1}) \\ \boldsymbol{\mu}_3^{k+1} = \boldsymbol{\mu}_3^k + \rho(\mathbf{F}_\Omega^{k+1} - \mathbf{Y}_\Omega + \mathbf{X}_\Omega^{k+1} + \mathcal{E}_\Omega^{k+1}) \end{cases}. \quad (9)$$

#### 1) X-subproblem

The X-subproblem in the Eq. (9) can be written as

$$\begin{aligned} \mathbf{X}^{k+1} = \arg \min_{\mathbf{X}} & \frac{\rho}{2} \left\| \mathbf{W}^k - \mathbf{X} + \frac{\boldsymbol{\mu}_1^k}{\rho} \right\|_F^2 \\ & + \frac{\rho}{2} \left\| \mathbf{F}_\Omega^k - (\mathbf{Y}_\Omega - \mathbf{X}_\Omega - \mathcal{E}_\Omega^k) + \frac{\boldsymbol{\mu}_3^k}{\rho} \right\|_F^2. \end{aligned} \quad (10)$$

The Eq. (10) can be simplified as

$$\mathbf{X}^{k+1} = \arg \min_{\mathbf{X}} \frac{\rho}{2} \|\mathbf{X} - \mathbf{N}\|_F^2 + \frac{\rho}{2} \|\mathbf{X}_\Omega - \mathbf{K}_\Omega\|_F^2, \quad (11)$$

where  $\mathbf{N} = \mathbf{W}^k + \frac{\boldsymbol{\mu}_1^k}{\rho}$  and  $\mathbf{K}_\Omega = \mathbf{Y}_\Omega - \mathbf{F}_\Omega^k - \mathcal{E}_\Omega^k - \frac{\boldsymbol{\mu}_3^k}{\rho}$ .

Solving the above formula yields,

$$\mathbf{X}^{k+1} = \mathbf{N}_{\Omega^c} + \frac{\mathbf{K}_\Omega + \mathbf{N}_\Omega}{2}. \quad (12)$$

#### 2) W-subproblem

The  $\mathbf{W}$ -subproblem in the Eq. (9) can be written as

$$\mathbf{W}^{k+1} = \arg \min_{\mathbf{W}} \alpha R(\mathbf{W}) + \frac{\rho}{2} \left\| \mathbf{W} - \mathbf{X}^{k+1} + \frac{\boldsymbol{\mu}_1^k}{\rho} \right\|_F^2, \quad (13)$$

where  $R(\mathbf{W})$  is an approximate function of the rank function. Using the proximal operator, the minimization problem can be succinctly expressed as follows,

$$\mathbf{W}^{k+1} = \arg \min_{\mathbf{W}} \text{Prox}_{\alpha\rho R} \left( \mathbf{X}^{k+1} - \frac{\boldsymbol{\mu}_1^k}{\rho} \right). \quad (14)$$

Finally, based on the Von-Neuman trace inequality [49], we obtain the relevant conclusion of the singular value contraction (see Theorem 4). And the closed-form solution of the above problem is easy to obtain.

**Lemma 1** (Von-Neuman Trace Inequality [49]). *Given two matrices  $\mathbf{M} = \mathbf{U}_M \mathbf{S}_M \mathbf{V}_M^T$ ,  $\mathbf{N} = \mathbf{Q}_N \boldsymbol{\Sigma}_N \mathbf{R}_N^T$ , where  $\mathbf{M}, \mathbf{N} \in \mathbb{R}^{n_1 \times n_2}$ ,  $\mathbf{S}_M = \text{diag}(s_1(\mathbf{M}), s_2(\mathbf{M}), \dots, s_r(\mathbf{M}))$ , and  $\boldsymbol{\Sigma}_N = \text{diag}(\sigma_1(\mathbf{N}), \sigma_2(\mathbf{N}), \dots, \sigma_r(\mathbf{N}))$ . Then they satisfy  $\text{tr}(\mathbf{M}^T \mathbf{N}) \leq \text{tr}(s(\mathbf{M})^T \sigma(\mathbf{N}))$ , where  $s(\mathbf{M})$  and  $\sigma(\mathbf{N})$  are the descending singular values of  $\mathbf{M}$  and  $\mathbf{N}$ , respectively.*

**Theorem 4.** *Consider a minimization problem of the following form,*

$$\min_{\mathbf{W}} \lambda \sum_{i=1}^{\min\{n_1, n_2\}} \psi(\sigma_i) + \frac{\rho}{2} \|\mathbf{W} - \mathbf{D}\|_F^2, \quad (15)$$

where  $\psi$  a smooth function,  $\mathbf{W}, \mathbf{D} \in \mathbb{R}^{n_1 \times n_2}$ ,  $\sigma_i$  and  $s_i$  is the  $i$ -th singular value of  $\mathbf{W}$  and  $\mathbf{D}$ , respectively. Suppose that the singular value decomposition of  $\mathbf{D}$  is expressed as  $\mathbf{D} = \mathbf{Q}_D \mathbf{S}_D \mathbf{R}_D^T$ . Note that the solution of the above optimization problem (15) is  $\mathbf{W}^* = \mathbf{U}_W \boldsymbol{\Sigma}_W \mathbf{V}_W^T$ , where  $\mathbf{U}_W = \mathbf{Q}_D$ ,  $\mathbf{V}_W = \mathbf{R}_D$ , and  $\boldsymbol{\Sigma}_W$  is a diagonal matrix composed of  $\sigma_i$ , which can be solved by the following problem

$$\min_{\sigma_i} \lambda \psi(\sigma_i) + \frac{\rho}{2} (\sigma_i - s_i)^2. \quad (16)$$

The proof of Theorem 4 is provided in Appendix C.

**Remark 3.** *In the literature [17] and [22], the optimal solutions of the two minimization problems are introduced in detail when  $R_1(\mathbf{W}) = \|\mathbf{W}\|_*$  and  $R_2(\mathbf{W}) = \|\mathbf{W}\|_{\text{Sp}, \tau}$ , respectively.*

### 3) $\mathcal{E}$ -subproblem

The  $\mathcal{E}$ -subproblem in the Eq. (9) can be expressed as

$$\begin{aligned} \mathcal{E}^{k+1} = \arg \min_{\mathcal{E}} \frac{\rho}{2} \left\| \mathbf{E}^k - \mathcal{E} + \frac{\boldsymbol{\mu}_2^k}{\rho} \right\|_F^2 \\ + \frac{\rho}{2} \left\| \mathbf{F}_\Omega^k - (\mathbf{Y}_\Omega - \mathbf{X}_\Omega^{k+1} - \mathcal{E}_\Omega) + \frac{\boldsymbol{\mu}_3^k}{\rho} \right\|_F^2. \end{aligned} \quad (17)$$

The above formula can be simplified as

$$\mathcal{E}^{k+1} = \arg \min_{\mathcal{E}} \frac{\rho}{2} \|\mathcal{E} - \mathbf{G}\|_F^2 + \frac{\rho}{2} \|\mathcal{E}_\Omega - \mathbf{B}_\Omega\|_F^2, \quad (18)$$

where  $\mathbf{G} = \mathbf{E}^k + \frac{\boldsymbol{\mu}_2^k}{\rho}$  and  $\mathbf{B}_\Omega = \mathbf{Y}_\Omega - \mathbf{X}_\Omega^{k+1} - \mathbf{F}_\Omega^k - \frac{\boldsymbol{\mu}_3^k}{\rho}$ . Solve the above formula can be obtained

$$\mathcal{E}^{k+1} = \mathbf{G}_{\Omega^c} + \frac{\mathbf{B}_\Omega + \mathbf{G}_\Omega}{2}. \quad (19)$$

### 4) $\mathbf{F}_\Omega$ -subproblem

## Algorithm 2 Low-rank matrix completion with OGER (5)

**Input:**  $\alpha, \lambda, \mathbf{Y}_\Omega, N, K$  and  $\rho > 0$ .

1: Initialize  $\mathbf{X}, \mathbf{W}, \mathcal{E}, \mathbf{F}_\Omega, \mathbf{E}, \boldsymbol{\mu}_1, \boldsymbol{\mu}_2, \boldsymbol{\mu}_3$  and  $k = 0$ .

2: **while** not converged **do**

3: Update  $\mathbf{X}^{k+1}$  by (12);

4: Update  $\mathbf{W}^{k+1}$  by (14);

5: Update  $\mathcal{E}^{k+1}$  by (19);

6: Update  $\mathbf{F}_\Omega^{k+1}$  by (21);

7: Update  $\mathbf{E}^{k+1}$  by (23);

8: Update  $\boldsymbol{\mu}_1^{k+1}, \boldsymbol{\mu}_2^{k+1}$  and  $\boldsymbol{\mu}_3^{k+1}$  by (24), (25) and (26);

9:  $\mathbf{Y}^{k+1} = \mathbf{X}^{k+1} + \mathcal{E}^{k+1}$ ;

10:  $k = k + 1$ .

11: **end while**

**Output:**  $\mathbf{Y}^* = \mathbf{Y}^{k+1}$ .

The  $\mathbf{F}_\Omega$ -subproblem in the Eq. (9) can be written as

$$\begin{aligned} \mathbf{F}_\Omega^{k+1} = \arg \min_{\mathbf{F}_\Omega} \frac{1}{2} \|\mathbf{F}_\Omega\|_F^2 \\ + \frac{\rho}{2} \left\| \mathbf{F}_\Omega - (\mathbf{Y}_\Omega - \mathbf{X}_\Omega^{k+1} - \mathcal{E}_\Omega^{k+1}) + \frac{\boldsymbol{\mu}_3^k}{\rho} \right\|_F^2. \end{aligned} \quad (20)$$

Solving the above formula yields

$$\mathbf{F}_\Omega^{k+1} = \frac{\rho (\mathbf{Y}_\Omega - \mathbf{X}_\Omega^{k+1} - \mathcal{E}_\Omega^{k+1}) - \boldsymbol{\mu}_3^k}{1 + \rho}. \quad (21)$$

### 5) $\mathbf{E}$ -subproblem

The  $\mathbf{E}$ -subproblem in the Eq. (9) can be written as

$$\mathbf{E}^{k+1} = \arg \min_{\mathbf{E}} \lambda \phi(\mathbf{E}) + \frac{\rho}{2} \left\| \mathbf{E} - \mathcal{E}^{k+1} + \frac{\boldsymbol{\mu}_2^k}{\rho} \right\|_F^2. \quad (22)$$

Using MM algorithm, the optimal solution of the problem is

$$\mathbf{E}^{k+1} = \left( \mathbf{I} + \frac{\lambda \boldsymbol{\Lambda}(\mathbf{E}^k)^T \boldsymbol{\Lambda}(\mathbf{E}^k)}{\rho} \right)^{-1} \mathbf{D}^k, \quad (23)$$

where  $\mathbf{D}^k = \mathcal{E}^{k+1} + \frac{\boldsymbol{\mu}_2^k}{\rho}$ ,  $\boldsymbol{\Lambda}(\mathbf{E}^k)$  is a diagonal matrix, and the elements on its diagonal are expressed as

$$[\boldsymbol{\Lambda}(\mathbf{E}^k)]_{l,l} = \sqrt{\sum_{i,j=-m_1}^{m_2} \left[ \sum_{k_1, k_2=-m_1}^{m_2} |\mathbf{E}^k_{r-i+k_1, i-j+k_2}|^2 \right]^{-1/2}}.$$

The detailed solution process of the minimization problem is provided in Appendix D.

### 6) Updating Lagrangian multipliers

Finally, the Lagrangian multipliers are updated as follows,

$$\boldsymbol{\mu}_1^{k+1} = \boldsymbol{\mu}_1^k + \rho (\mathbf{W}^{k+1} - \mathbf{X}^{k+1}), \quad (24)$$

$$\boldsymbol{\mu}_2^{k+1} = \boldsymbol{\mu}_2^k + \rho (\mathbf{E}^{k+1} - \mathcal{E}^{k+1}), \quad (25)$$

$$\boldsymbol{\mu}_3^{k+1} = \boldsymbol{\mu}_3^k + \rho (\mathbf{F}_\Omega^{k+1} - \mathbf{Y}_\Omega + \mathbf{X}_\Omega^{k+1} + \mathcal{E}_\Omega^{k+1}). \quad (26)$$

**Remark 4.** *The algorithm framework of the proposed model is shown in Algorithm 2. The main cost of Algorithm 2 lies in computing  $\mathbf{W}$  and  $\mathcal{E}$  subproblems when the ADMM framework is iterated once. In  $\mathbf{W}$  subproblem, the complexity is mainly from computing the SVD and the shrinkage operator, whose computational costs are  $O(\min\{n_1^2 n_2, n_1 n_2^2\})$  and  $O(\min\{n_1, n_2\})$ , respectively. In  $\mathcal{E}$  subproblem, the complexity is mainly from computing the overlapping blocks*

of the matrix and the number of inner turns  $N$ , and their total computational cost is  $O(Nn_1n_2)$ . Therefore, the computational cost at each iteration of Algorithm 2 is  $O(\min\{n_1^2n_2, n_1n_2^2\} + Nn_1n_2)$ .

#### IV. NUMERICAL EXPERIMENTS

In this section, to verify the effectiveness and superiority of the proposed low-rank matrix completion model with overlapping group error representation for image recovery, we choose two approximate representations of the rank function,  $R_1$  [17] and  $R_2$  [22]. At this point, the model (5) is described in detail as

$$\begin{aligned} \min_{\mathbf{X}, \mathcal{E}} \|\mathbf{X}\|_* + \lambda\phi(\mathcal{E}) \quad s.t. \quad \mathbf{Y}_\Omega = \mathbf{X}_\Omega + \mathcal{E}_\Omega. \\ \min_{\mathbf{X}, \mathcal{E}} \|\mathbf{X}\|_{S_{p,\tau}} + \lambda\phi(\mathcal{E}) \quad s.t. \quad \mathbf{Y}_\Omega = \mathbf{X}_\Omega + \mathcal{E}_\Omega. \end{aligned}$$

We compare the two new models with four other classical models, including the nuclear norm minimization (NNM) model [17], the weighted Schatten  $p$  norm minimization (WSP) model [25], the Schatten capped  $p$  (SCP) method [22], and the ratio of the nuclear norm and the Frobenius norm (N/F) method [27]. We conducted a series of matrix completion experiments under identical conditions to assess the image recovery capabilities of these six models. All experiments were performed on a computer equipped with a Windows 10 operating system and an Intel Core i5-8250U running at 1.80 GHz and completed using MATLAB (R2014a version) software.

Fig. 4 presents 12 test images, which have been widely used for assessing the effects of image recovery across various models due to their low-rank nature. To evaluate the recovery effect of the models more effectively, two objective evaluation metrics, peak signal-to-noise ratio (PSNR) and signal-to-noise ratio (SNR) are employed for the experimental results. The definitions of PSNR and SNR are as follows,

$$\begin{aligned} \text{PSNR} &= 10 \cdot \log_{10} \left( \frac{n_1 n_2}{\|\mathbf{Y} - \mathbf{Y}^*\|_F^2} \right), \\ \text{SNR} &= 10 \cdot \log_{10} \left( \frac{\|\mathbf{Y}\|_F^2}{\|\mathbf{Y} - \mathbf{Y}^*\|_F^2} \right). \end{aligned}$$

In the numerical experiments, the higher the PSNR and SNR values relative to each other, the better the recovered image. The bold font indicates the optimal value. The ratio between the observed matrix elements and the total number of elements in the entire matrix is expressed using the sampling rate  $\eta$ , which is defined as

$$\eta = 1 - \frac{\text{num}(\mathbf{Y}_\Omega)}{\text{num}(\mathbf{Y})},$$

where  $\text{num}(\cdot)$  denotes the number of entries in the matrix. Furthermore, the iterative stopping condition of the modeling algorithm is set to ensure that the relative error (RE) of the recovered image in two consecutive iterations is less than the



Fig. 4: Test images for numerical experiments.

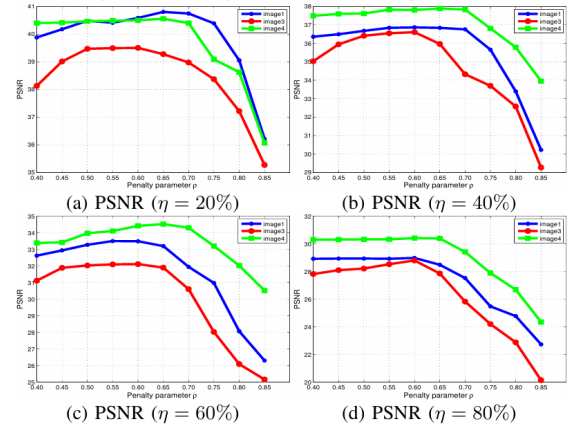


Fig. 5: The PSNR values of the test images (‘image1’, ‘image3’ and, ‘image4’) are restored by different penalty parameter  $\rho$  values.

preset accuracy. Here, the preset accuracy is set to  $tol = 10^{-5}$ ,

$$RE = \frac{\|\mathbf{Y}^k - \mathbf{Y}^{k-1}\|_F^2}{\|\mathbf{Y}^k\|_F^2} \leq tol.$$

##### A. Discussion of Related Parameters

In this subsection, we delve into the parameters of the model in detail. Note that, we choose the surrogate function  $R_2$  to represent the low-rank component within the model. The parameters under discussion primarily encompass the penalty parameter  $\rho$ , as well as the iteration number  $N$  and the group size  $K$  in the overlapping group subproblem (22).

1) *Penalty parameter  $\rho$* : We selected ‘image1’, ‘image3’, and ‘image4’ as test images and applied random loss masks with values of  $\eta = 20\%$ ,  $40\%$ ,  $60\%$ ,  $80\%$ . The parameter  $\rho$  was varied within the range of  $[0.4, 0.85]$  in increments of  $0.05$ , while the remaining parameters remained fixed. Fig. 5 illustrates the variation of the PSNR values across different values of  $\rho$ . We observed that the highest PSNR was achieved when  $\rho = 0.6$ . Therefore, we set  $\rho = 0.6$  for the subsequent experiments.

2) *Iteration number  $N$* : We select the test images including ‘image4’-‘image9’, to which a text mask 2 has been applied. We set  $N = 1, 3, 5, 10, 30, 50$  while keeping other parameters constant. The resulting PSNR and SNR values for the recovered images are presented in Table I. From Table I, it can be observed that as  $N$  increases from 1 to 5, the PSNR and SNR values gradually increase. However, once  $N$  exceeds 5, the PSNR and SNR values remain largely unchanged. Consequently, to avoid the additional time expenditure associated

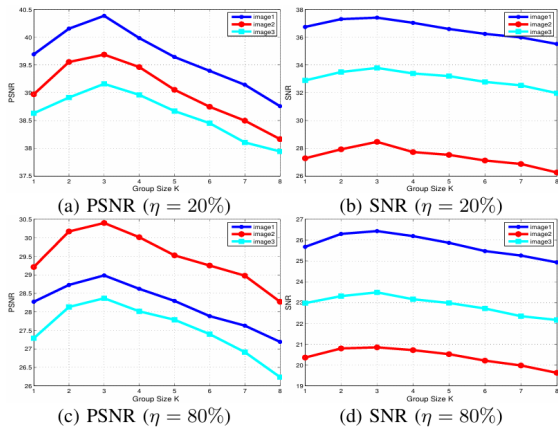


Fig. 6: The PSNR and SNR values of the test images (‘image1’, ‘image2’, and ‘image3’) are restored by different group size  $K$  values.

with excessive iterations, we set  $N = 5$  for the subsequent experiments.

3) *Group size  $K$* : We selected ‘image1’, ‘image2’, and ‘image3’ as test images and applied a random loss mask with values of  $\eta = 20\%$  and  $\eta = 80\%$ . The parameter  $K$  was varied within the range of  $[1, 8]$  in increments of 1, while the remaining parameters remained fixed. Fig. 6 illustrates the functional relationship between the PSNR and SNR values of the restored images and various values of  $K$ . It is important to note that when  $K = 1$ , the overlapping group sparsity metric reduces to a point sparsity metric. We observed that the proposed model achieved the best numerical results when  $K = 3$ . Therefore, we set  $K = 3$  for subsequent experiments.

Furthermore, other parameters within the model were manually adjusted to achieve a more optimal recovery outcome. The regularization parameters were set to  $\alpha \in [0.1, 5]$  and  $\lambda \in [0.01, 1]$ .

## B. Random Mask Experiments

In this subsection, the recovery effect of the proposed model is validated with the addition of random masks. We apply masks with randomly missing entries of  $\eta = 20\%$ ,  $40\%$ ,  $60\%$ ,  $80\%$  to the test images and present the recovered PSNR and SNR values of the six models in Table II. The numerical results in Table II indicate that the proposed model outperforms the other models. Due to space limitations, Fig. 7 shows only a selection of the recovered images. It can be observed that as the number of missing entries in the image increases, the recovery effect of the model decreases. When the missing entries reached  $80\%$ , the SCP model and the N/F model left a small amount of mask noise in the recovered image, in contrast to the proposed model. Consequently, the numerical results and subjective visualization both demonstrate that the proposed model outperforms the other competing models in terms of recovery.

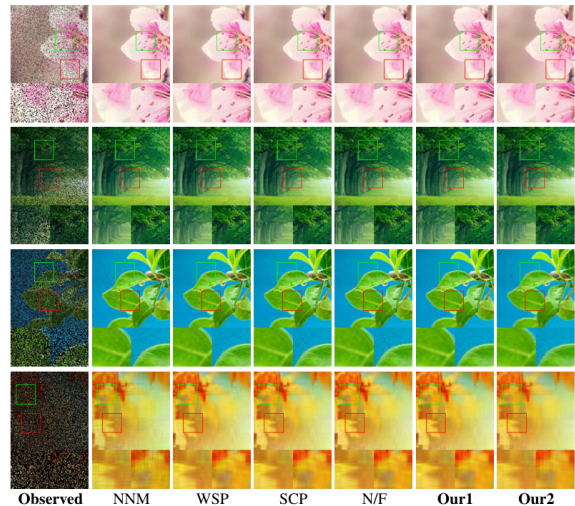


Fig. 7: The restored results of different models for random mask experiments.

## C. Text Mask Experiments

To further verify the effectiveness of the proposed model in recovering important information, such as details and textures, we recover images with added text masks in this subsection. The numerical results of the recovered images for the six models are shown in Table III. The results indicate that the proposed model is capable of achieving optimal recovery outcomes compared to other competing models. Fig. 8 shows only a selection of the recovered images from Table III. The numerical results and the quality of the recovered images using the proposed model 1 are demonstrably superior to those of the NNM model. Some of the images are recovered to a higher standard than those of the WSP model. This suggests that the proposed model, which incorporates overlapping group error characterization, exhibits superior performance.

## D. Block Mask Experiments

This subsection aims to corroborate the efficacy of the proposed model in addressing the challenges posed by extensive missing data in images. To achieve this, we conduct recovery experiments on images with added block masks. Table IV illustrates the recovery of PSNR and SNR values for six models, with corresponding results presented in Fig. 9.

The significant data loss in the image resulting from the application of the block mask poses a substantial challenge to the models’ ability to recover the original information. For instance, when the triangular block mask is incorporated, the NNM model and the WSP model result in the formation of substantial black blocks in the central region of the recovered image, while the SCP model and the N/F model are unable to fully recover the intricate details of the tree branches when the large pentagram mask is employed. In contrast, the recovered images from the proposed model appear more naturalistic. Furthermore, Fig. 10 illustrates localized slices of ‘image9’-‘image12’ in their 200th column after recovery. It can be seen that the proposed model produces the most effective results.

TABLE I: The PSNR and SSIM values for different  $N$  values with text mask 2.

$N$ Image	$N = 1$		$N = 3$		$N = 5$		$N = 10$		$N = 30$		$N = 50$	
	PSNR	SNR	PSNR	SNR	PSNR	SNR	PSNR	SNR	PSNR	SNR	PSNR	SNR
image4	39.0170	29.6185	39.1890	29.8357	39.3219	30.1686	39.3119	30.1597	39.3075	30.1492	39.3008	30.1416
image5	37.0144	31.4921	37.1419	31.6133	37.3028	31.7674	37.3101	31.7732	37.3943	31.7580	37.2722	31.7365
image6	40.1568	33.7584	40.3102	33.9193	40.4613	34.0681	40.4698	34.1057	40.4574	34.0926	40.4229	34.0772
image7	40.0822	31.5669	40.1731	31.7562	40.3174	37.8480	40.3029	37.8296	40.2881	37.8012	40.2763	37.7949
image8	40.3058	34.5012	40.4918	34.6716	40.6893	34.8816	40.6914	34.8922	40.6830	34.8675	40.6715	34.8534
image9	39.3870	34.5911	39.6375	34.7445	39.7685	34.9089	39.7613	34.8971	39.7524	34.8783	39.7316	34.8608

TABLE II: The PSNR and SNR values of all methods with different random masks.

Methods Image	mask	NNM		WSP		SCP		N/F		Our1		Our2	
		PSNR	SNR	PSNR	SNR								
image1	random mask 20%	36.18	32.92	38.40	35.29	39.77	36.62	40.26	37.24	38.69	35.54	<b>40.38</b>	<b>37.41</b>
	random mask 40%	32.58	29.31	34.14	31.75	35.04	32.80	35.93	33.12	34.58	32.05	<b>36.62</b>	<b>33.87</b>
	random mask 60%	29.12	26.56	31.27	27.98	32.25	29.16	32.65	29.42	31.65	28.18	<b>33.04</b>	<b>30.06</b>
	random mask 80%	24.57	22.19	26.30	24.92	27.97	25.64	28.42	26.08	26.89	25.27	<b>28.98</b>	<b>26.41</b>
image2	random mask 20%	35.50	24.75	37.74	26.35	38.90	27.98	39.45	28.20	37.81	26.42	<b>39.69</b>	<b>28.63</b>
	random mask 40%	32.98	22.06	34.01	23.52	35.56	24.28	35.91	24.93	34.44	23.62	<b>36.48</b>	<b>25.42</b>
	random mask 60%	29.87	20.10	31.39	21.57	32.43	22.32	32.86	22.79	31.58	21.43	<b>33.32</b>	<b>23.14</b>
	random mask 80%	26.17	17.29	28.62	19.16	29.87	20.13	30.04	20.22	28.97	19.65	<b>30.40</b>	<b>20.89</b>
image3	random mask 20%	35.21	30.85	37.24	32.02	38.43	32.95	38.87	33.12	37.60	32.57	<b>39.15</b>	<b>33.78</b>
	random mask 40%	32.68	26.05	33.99	28.61	35.08	29.72	35.22	29.85	34.13	28.95	<b>36.62</b>	<b>30.54</b>
	random mask 60%	29.09	24.13	30.60	24.86	31.15	25.58	31.43	25.96	30.92	25.38	<b>32.04</b>	<b>26.91</b>
	random mask 80%	25.46	19.09	27.45	21.91	27.96	22.87	28.12	23.06	27.83	22.16	<b>28.67</b>	<b>23.48</b>
image4	random mask 20%	36.69	27.25	38.76	29.33	39.40	30.05	39.64	30.26	39.03	29.60	<b>40.06</b>	<b>30.91</b>
	random mask 40%	34.00	24.09	35.56	26.48	36.82	27.53	37.06	28.02	35.74	26.59	<b>37.67</b>	<b>28.50</b>
	random mask 60%	30.81	22.13	32.25	23.49	33.97	24.89	34.15	25.03	32.39	23.73	<b>34.74</b>	<b>25.58</b>
	random mask 80%	26.23	18.04	27.98	19.96	29.43	21.62	29.43	21.74	28.15	20.21	<b>30.25</b>	<b>22.06</b>

TABLE III: The PSNR and SNR values of all methods with different text masks.

Methods Image	mask	NNM		WSP		SCP		N/F		Our1		Our2	
		PSNR	SNR	PSNR	SNR								
image4	text mask1	35.14	26.81	37.77	28.61	38.68	29.42	39.09	29.66	38.02	28.94	<b>39.32</b>	<b>30.16</b>
	text mask2	35.36	27.29	37.82	28.76	38.84	29.93	39.22	30.03	38.33	29.12	<b>39.51</b>	<b>30.24</b>
	text mask3	35.22	26.93	37.80	28.72	38.79	29.78	39.15	29.82	38.19	28.99	<b>39.35</b>	<b>30.20</b>
image5	text mask1	33.14	28.06	35.39	29.86	36.93	31.27	37.01	31.43	35.54	30.05	<b>37.29</b>	<b>31.76</b>
	text mask2	35.42	29.89	37.21	31.68	38.16	32.63	38.32	32.79	37.52	31.99	<b>38.54</b>	<b>33.02</b>
	text mask3	33.82	28.31	35.94	30.41	37.72	32.19	37.96	32.43	36.09	30.56	<b>38.13</b>	<b>32.60</b>
image6	text mask1	36.34	29.85	38.47	32.02	39.66	33.28	40.14	33.56	38.55	32.10	<b>40.47</b>	<b>34.02</b>
	text mask2	37.23	30.78	39.58	33.04	40.52	34.08	41.07	34.62	39.63	33.49	<b>41.45</b>	<b>35.01</b>
	text mask3	37.08	30.63	39.34	32.89	40.34	33.95	40.82	34.37	39.86	33.42	<b>41.23</b>	<b>34.78</b>
image7	text mask1	36.03	33.56	38.85	36.38	39.46	36.98	39.89	37.42	39.11	36.64	<b>40.32</b>	<b>37.85</b>
	text mask2	37.36	34.92	39.77	37.10	40.43	37.96	40.73	38.27	39.90	37.41	<b>41.39</b>	<b>38.93</b>
	text mask3	37.35	34.88	39.45	36.99	40.26	37.79	40.60	38.13	39.68	37.23	<b>41.18</b>	<b>38.71</b>
image8	text mask1	37.23	31.44	39.02	32.23	40.04	34.25	40.21	34.42	39.32	33.53	<b>40.67</b>	<b>34.88</b>
	text mask2	37.64	31.85	39.93	34.14	41.22	35.42	41.56	35.77	40.51	34.71	<b>41.87</b>	<b>36.08</b>
	text mask3	37.33	31.54	39.51	33.72	40.99	35.21	41.36	35.57	40.12	34.33	<b>41.62</b>	<b>35.83</b>
image9	text mask1	36.20	31.33	38.65	33.79	39.17	34.31	39.41	34.54	39.98	34.11	<b>39.77</b>	<b>34.91</b>
	text mask2	36.83	31.97	38.88	34.01	39.89	35.03	40.27	35.36	39.35	34.48	<b>40.43</b>	<b>35.57</b>
	text mask3	36.60	31.62	38.71	33.85	39.31	34.45	39.71	34.85	39.05	34.30	<b>40.00</b>	<b>35.14</b>

TABLE IV: The PSNR and SNR values of all methods with different block masks.

Methods Image	mask	NNM		WSP		SCP		N/F		Our1		Our2	
		PSNR	SNR	PSNR	SNR								
image8	block mask1	32.37	24.58	34.26	28.47	35.01	29.22	35.29	29.50	34.68	28.89	<b>35.63</b>	<b>29.85</b>
	block mask2	25.09	19.31	27.15	21.36	28.40	22.61	28.86	23.03	27.77	21.98	<b>29.04</b>	<b>23.21</b>
	block mask3	28.69	22.90	30.93	25.08	31.76	25.91	31.97	26.19	31.37	25.58	<b>32.35</b>	<b>26.56</b>
	block mask4	29.95	24.13	32.15	26.34	32.52	26.76	32.81	27.02	31.85	26.02	<b>33.01</b>	<b>27.24</b>
	block mask5	20.01	14.28	22.29	16.33	23.17	17.32	23.64	17.87	22.66	16.86	<b>23.87</b>	<b>18.05</b>
image9	block mask1	31.79	26.61	33.95	28.89	34.85	29.99	35.06	30.19	34.41	29.54	<b>35.42</b>	<b>30.25</b>
	block mask2	24.60	19.74	26.94	22.07	27.96	23.10	28.19	23.33	27.32	22.46	<b>28.44</b>	<b>23.57</b>
	block mask3	28.29	23.12	30.64	25.41	31.54	26.37	32.08	26.91	30.95	25.78	<b>32.42</b>	<b>27.23</b>
	block mask4	30.00	25.13	32.62	27.45	33.42	28.26	33.85	28.67	33.21	28.04	<b>34.02</b>	<b>28.84</b>
	block mask5	17.53	12.57	19.95	14.88	21.06	15.89	21.54	16.37	20.54	15.33	<b>21.88</b>	<b>16.71</b>
image10	block mask1	28.31	26.39	30.07	28.16	34.62	32.71	35.00	33.09	34.32	32.40	<b>35.34</b>	<b>33.41</b>
	block mask2	24.94	19.28	27.36	22.41	28.09	23.18	28.46	23.55	27.89	22.92	<b>28.87</b>	<b>22.96</b>
	block mask3	25.69	23.75	28.97	27.02	29.65	27.74	29.88	27.97	29.31	27.43	<b>30.13</b>	<b>27.25</b>
	block mask4	28.13	26.22	30.50	28.59	31.45	29.54	31.77	29.85	31.04	29.12	<b>32.00</b>	<b>30.88</b>
	block mask5	14.94	11.02	17.35	15.01	19.13	17.26	19.59	17.68	18.85	16.91	<b>19.76</b>	<b>17.85</b>
image11	block mask1	27.12	25.10	30.43	28.42	31.01	28.97	31.35	29.33	30.70	28.69	<b>31.56</b>	<b>29.54</b>
	block mask2	21.94	17.86	24.05	20.98	24.87	21.88	25.12	22.10	24.32	21.29	<b>25.45</b>	<b>22.44</b>
	block mask3	25.03	23.09	27.87	25.80	28.48	26.46	28.80	26.78	28.04	26.02	<b>29.13</b>	<b>27.17</b>
	block mask4	26.76	24.75	29.51	27.49	30.24	28.21	30.65	28.62	29.92	27.90	<b>30.89</b>	<b>28.93</b>
	block mask5	13.19	11.23	16.28	13.56	17.11	14.47	17.43	14.86	16.73	14.02	<b>17.77</b>	<b>15.08</b>
image12	block mask1	36.67	30.04	38.48	32.49	39.64	33.08	39.96	33.35	38.74	32.88	<b>40.23</b>	<b>33.63</b>
	block mask2	35.87	28.23	37.37	30.74	38.01	31.41	38.40	31.80	37.65	31.04	<b>38.82</b>	<b>32.22</b>
	block mask3	35.99	29.40	38.03	31.36	39.07	32.47	39.59	32.99	38.63	32.02	<b>39.83</b>	<b>33.23</b>
	block mask4	35.73	28.12	37.95	30.42	38.93	32.34	39.35	32.76	38.52	31.91	<b>39.59</b>	<b>32.99</b>
	block mask5	34.39	27.70	36.28	29.67	37.31	30.71	37.83	31.25	36.73	30.13	<b>38.28</b>	<b>31.64</b>

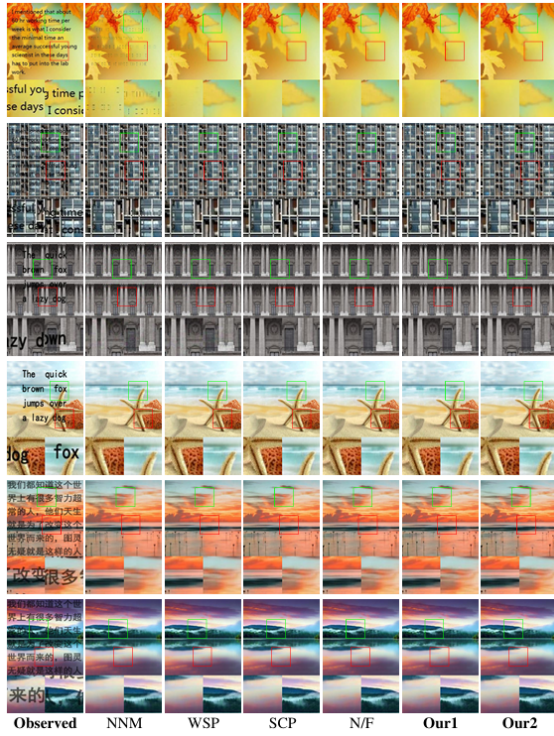


Fig. 8: The restored results of different models for text mask experiments.

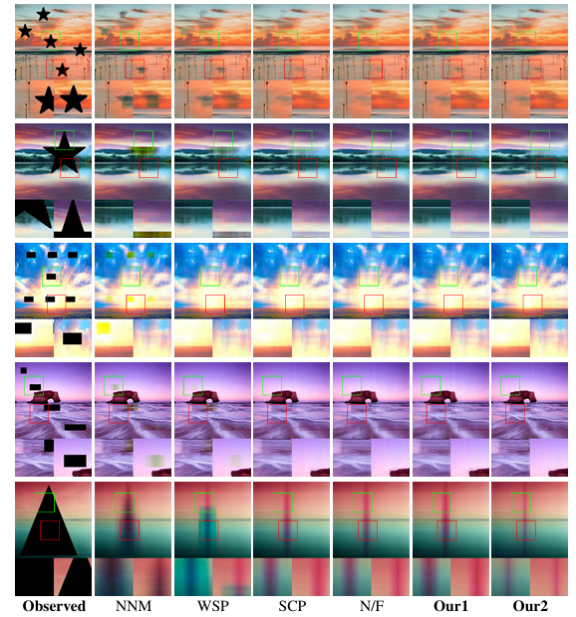


Fig. 9: The restored results of different models for block mask experiments.

### E. Convergence Analysis

In this subsection, to verify the convergence of Algorithm 2, we select the ‘image9’ and ‘image12’ with the block masks 3 and masks 4 as test images. Fig. 11 illustrates the functional relationship between the recovered PSNR, SNR, and RE values and the number of iterations.

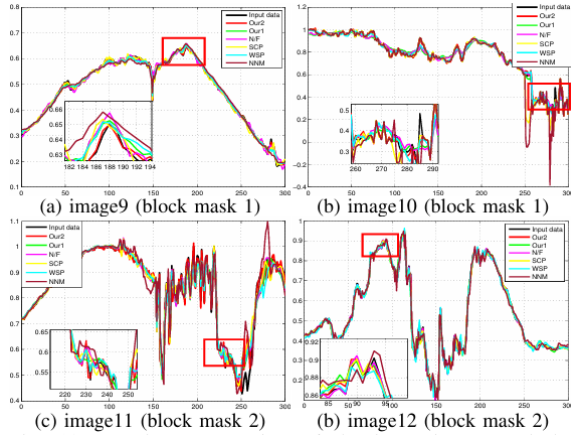


Fig. 10: Local cross-section of the input image and the restored image.

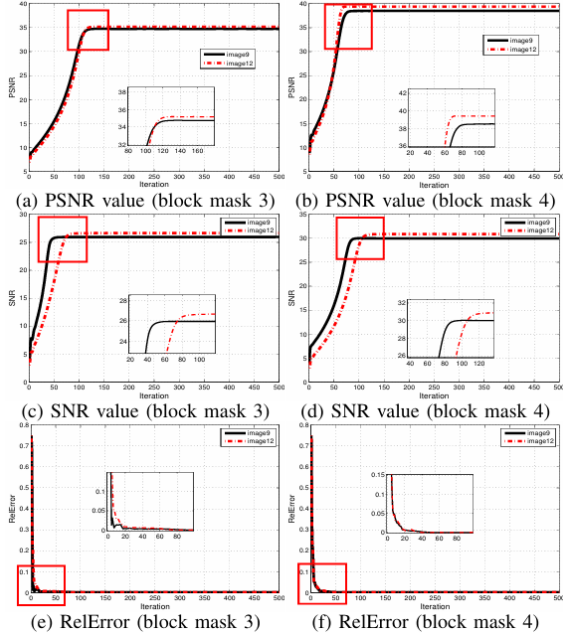


Fig. 11: Convergence of the proposed model for different block masks.

Observing Fig. 11 reveals that the PSNR and SNR values gradually increase and stabilize as the number of iterations increases, while the RE value decreases rapidly and tends towards zero. Thus, the experimental results validate the convergence of Algorithm 2.

Furthermore, to delve deeply into the convergence properties of Algorithm 2, we conduct a rigorous numerical verification. We first make the following fundamental assumptions regarding the objective functions in the minimization problem (10).

**Assumption 1.** The functions  $R(\mathbf{W})$  and  $\phi(\mathbf{E})$  are closed and lower semi-continuous within their respective domains, and their gradient functions satisfy the Lipschitz continuity condition. Specifically, there exist positive constants  $S_1$  and  $S_2$  such that for any  $x_1, x_2$  in the domain of  $R(\mathbf{W})$  and any

$x_3, x_4$  in the domain of  $\phi(\mathbf{E})$ , it holds that

$$\begin{aligned} \|\nabla R(x_1) - \nabla R(x_2)\|_F &\leq S_1 \|x_1 - x_2\|_F, \\ \|\nabla \phi(x_3) - \nabla \phi(x_4)\|_F &\leq S_2 \|x_3 - x_4\|_F. \end{aligned}$$

**Assumption 2.** The objective function  $R(\mathbf{W}) + \phi(\mathbf{E})$  is bounded below.

**Theorem 5.** Let  $\{\Gamma^k\}_{k=1}^{+\infty}$  be the sequence generated by Algorithm 2, then there must exist positive constants  $c_1$  and  $c_2$  such that the following inequality holds,

$$\begin{aligned} &L(\mathbf{X}^{k+1}, \mathbf{W}^k, \mathcal{E}^k, \mathbf{F}_\Omega^k, \mathbf{E}^k, \mu_1^k, \mu_2^k, \mu_3^k) \\ &- L(\mathbf{X}^k, \mathbf{W}^k, \mathcal{E}^k, \mathbf{F}_\Omega^k, \mathbf{E}^k, \mu_1^k, \mu_2^k, \mu_3^k) \\ &\leq -c_1 \|\mathbf{X}^{k+1} - \mathbf{X}^k\|_F^2 - c_2 \|\mathbf{X}_\Omega^{k+1} - \mathbf{X}_\Omega^k\|_F^2. \end{aligned} \quad (27)$$

**Theorem 6.** Let  $\{\Gamma^k\}_{k=1}^{+\infty}$  be the sequence generated by Algorithm 2, then there must exist a positive constant  $c_3$  such that the following inequality holds,

$$\begin{aligned} &L(\mathbf{X}^{k+1}, \mathbf{W}^{k+1}, \mathcal{E}^k, \mathbf{F}_\Omega^k, \mathbf{E}^k, \mu_1^k, \mu_2^k, \mu_3^k) \\ &- L(\mathbf{X}^{k+1}, \mathbf{W}^k, \mathcal{E}^k, \mathbf{F}_\Omega^k, \mathbf{E}^k, \mu_1^k, \mu_2^k, \mu_3^k) \\ &\leq -\alpha c_3 \|\mathbf{W}^{k+1} - \mathbf{W}^k\|_F^2. \end{aligned} \quad (28)$$

**Theorem 7.** Let  $\{\Gamma^k\}_{k=1}^{+\infty}$  be the sequence generated by Algorithm 2, then there must exist positive constants  $c_4, c_5, c_6$  and  $c_7$  such that the following inequality holds,

$$\begin{aligned} &L(\mathbf{X}^{k+1}, \mathbf{W}^{k+1}, \mathcal{E}^{k+1}, \mathbf{F}_\Omega^k, \mathbf{E}^k, \mu_1^k, \mu_2^k, \mu_3^k) \\ &- L(\mathbf{X}^{k+1}, \mathbf{W}^{k+1}, \mathcal{E}^k, \mathbf{F}_\Omega^k, \mathbf{E}^k, \mu_1^k, \mu_2^k, \mu_3^k) \\ &\leq -c_4 \|\mathcal{E}^{k+1} - \mathcal{E}^k\|_F^2 - c_5 \|\mathcal{E}_\Omega^{k+1} - \mathcal{E}_\Omega^k\|_F^2, \end{aligned} \quad (29)$$

$$\begin{aligned} &L(\mathbf{X}^{k+1}, \mathbf{W}^{k+1}, \mathcal{E}^{k+1}, \mathbf{F}_\Omega^{k+1}, \mathbf{E}^k, \mu_1^k, \mu_2^k, \mu_3^k) \\ &- L(\mathbf{X}^{k+1}, \mathbf{W}^{k+1}, \mathcal{E}^{k+1}, \mathbf{F}_\Omega^k, \mathbf{E}^k, \mu_1^k, \mu_2^k, \mu_3^k) \\ &\leq -c_6 \|\mathbf{F}_\Omega^{k+1} - \mathbf{F}_\Omega^k\|_F^2, \end{aligned} \quad (30)$$

$$\begin{aligned} &L(\mathbf{X}^{k+1}, \mathbf{W}^{k+1}, \mathcal{E}^{k+1}, \mathbf{F}_\Omega^{k+1}, \mathbf{E}^{k+1}, \mu_1^k, \mu_2^k, \mu_3^k) \\ &- L(\mathbf{X}^{k+1}, \mathbf{W}^{k+1}, \mathcal{E}^{k+1}, \mathbf{F}_\Omega^{k+1}, \mathbf{E}^k, \mu_1^k, \mu_2^k, \mu_3^k) \\ &\leq -\lambda c_7 \|\mathbf{E}^{k+1} - \mathbf{E}^k\|_F^2. \end{aligned} \quad (31)$$

**Theorem 8.** Let  $\{\Gamma^k\}_{k=1}^{+\infty}$  be the sequence generated by Algorithm 2, then there must exist positive constants  $c_8, c_9$  and  $c_{10}$  such that the following inequality holds,

$$\begin{aligned} &L(\mathbf{X}^{k+1}, \mathbf{W}^{k+1}, \mathcal{E}^{k+1}, \mathbf{F}_\Omega^{k+1}, \mathbf{E}^{k+1}, \mu_1^{k+1}, \mu_2^{k+1}, \mu_3^{k+1}) \\ &- L(\mathbf{X}^{k+1}, \mathbf{W}^{k+1}, \mathcal{E}^{k+1}, \mathbf{F}_\Omega^{k+1}, \mathbf{E}^k, \mu_1^k, \mu_2^k, \mu_3^k) \\ &\leq c_8 \|\mathbf{W}^{k+1} - \mathbf{W}^k\|_F^2 + c_9 \|\mathbf{E}^{k+1} - \mathbf{E}^k\|_F^2 \\ &\quad + c_{10} \|\mathbf{F}_\Omega^{k+1} - \mathbf{F}_\Omega^k\|_F^2. \end{aligned} \quad (32)$$

**Theorem 9.** Let  $\{\Gamma^k\}_{k=1}^{+\infty}$  be the sequence generated by Algorithm 2, and the penalty parameter  $\rho$  is large enough, such that when  $\rho \geq \max\left\{\frac{\alpha^2 S_1^2}{c_3}, \frac{\lambda^2 S_2^2}{c_7}, \frac{1}{c_6}\right\}$ , the following inequality holds,

$$\begin{aligned} &L(\mathbf{X}^{k+1}, \mathbf{W}^{k+1}, \mathcal{E}^{k+1}, \mathbf{F}_\Omega^{k+1}, \mathbf{E}^{k+1}, \mu_1^{k+1}, \mu_2^{k+1}, \mu_3^{k+1}) \\ &\leq L(\mathbf{X}^k, \mathbf{W}^k, \mathcal{E}^k, \mathbf{F}_\Omega^k, \mathbf{E}^k, \mu_1^k, \mu_2^k, \mu_3^k). \end{aligned} \quad (33)$$

**Theorem 10.** Let  $\{\Gamma^k\}_{k=1}^{+\infty}$  be the sequence generated by Algorithm 2, then the sequence is bounded.

**Theorem 11.** Let  $\{\Gamma^k\}_{k=1}^{+\infty}$  be the sequence generated by Algorithm 2, we have

$$\lim_{k \rightarrow +\infty} \|\Gamma^{k+1} - \Gamma^k\|_F^2 = 0. \quad (34)$$

**Theorem 12.** Let  $\{\Gamma^k\}_{k=1}^{+\infty}$  be the sequence generated by Algorithm 2, then any limit point  $\Gamma^*$  of the sequence, which is defined as  $\Gamma^* = (\mathbf{X}^*, \mathbf{W}^*, \mathcal{E}^*, \mathbf{F}_\Omega^*, \mathbf{E}^*, \mu_1^*, \mu_2^*, \mu_3^*)$ , is a stable point of the formula (8).

**Remark 5.** Based on the above assumptions and Theorems 5-12, it has been proven that the sequence  $\Gamma^k = L(\mathbf{X}^k, \mathbf{W}^k, \mathcal{E}^k, \mathbf{F}_\Omega^k, \mathbf{E}^k, \mu_1^k, \mu_2^k, \mu_3^k)$  generated by Algorithm 2 converges to a stable point  $\Gamma^* = L(\mathbf{X}^*, \mathbf{W}^*, \mathcal{E}^*, \mathbf{F}_\Omega^*, \mathbf{E}^*, \mu_1^*, \mu_2^*, \mu_3^*)$  of the augmented Lagrangian function  $L(\mathbf{X}, \mathbf{W}, \mathcal{E}, \mathbf{F}_\Omega, \mathbf{E}, \mu_1, \mu_2, \mu_3)$ . The detailed proofs of the theorems are provided in Appendices E-L.

## V. CONCLUSION

In this paper, we design a novel low-rank matrix decomposition architecture which assumes that the matrix consists of both low-rank and structured sparse components. On this basis, we propose a generalized low-rank matrix completion model with OGER. In our model, OGER employs the group sparsity metric to quantify the structured sparse elements within matrix data. This enhances the model's capacity to capture structural information, thereby improving its fitting capability and effectively preserving sparse details in the reconstructed matrix. Moreover, the proposed model is computationally solved by integrating the MM algorithm into the ADMM framework. To validate the efficacy of OGER, we conduct recovery experiments on images using random masks, text masks, and block masks. The experimental outcomes illustrate that our model surpasses alternative approaches in terms of matrix recovery performance. It is important to clarify that the current proposed model is designed specifically for low-rank matrix completion. In future research, our aim is to expand its capabilities to include tensor completion as well.

## ACKNOWLEDGEMENTS

This work was supported in part by the Natural Science Foundation of China under Grant No. 62061016 and 61561019, the Doctoral Scientific Fund Project of Hubei Minzu University under Grant No. MY2015B001, the Internal Scientific Research Project of Hubei Minzu University under Grant No. XN2305, and the Graduate Education Innovation Project of Hubei Minzu University under Grant No. MYK2024006 and STK2023002.

## REFERENCES

- [1] F. Nie, Z. Li, Z. Hu, R. Wang, and X. Li, "Robust matrix completion with column outliers," *IEEE Transactions on Cybernetics*, vol. 52, no. 11, pp. 12 042–12 055, 2021.
- [2] Q. Yao and J. Kwok, "Efficient learning with a family of nonconvex regularizers by redistributing nonconvexity," *Journal of Machine Learning Research*, vol. 18, no. 179, pp. 1–52, 2018.
- [3] X. Luo, M. Zhou, S. Li, L. Hu, and M. Shang, "Non-negativity constrained missing data estimation for high-dimensional and sparse matrices from industrial applications," *IEEE Transactions on Cybernetics*, vol. 50, no. 5, pp. 1844–1855, 2020.
- [4] Y. Yang and C. Ma, "Optimal tuning-free convex relaxation for noisy matrix completion," *IEEE Transactions on Information Theory*, vol. 69, no. 10, pp. 6571–6585, 2023.
- [5] B. Shi, F. Gu, Z. Pang, and Y. Zeng, "Remove the salt and pepper noise based on the high order total variation and the nuclear norm regularization," *Applied Mathematics and Computation*, vol. 421, p. 126925, 2022.
- [6] J. Yin, L. Gao, and Z. Zhang, "Scalable distributed nonnegative matrix factorization with block-wise updates," *IEEE Transactions on Knowledge and Data Engineering*, vol. 30, no. 6, pp. 1136–1149, 2018.
- [7] L. Chen, X. Jiang, X. Liu, and Z. Zhou, "Logarithmic norm regularized low-rank factorization for matrix and tensor completion," *IEEE Transactions on Image Processing*, vol. 30, pp. 3434–3449, 2021.
- [8] B. Shi, A. Tom, and S. George, "Simultaneous denoising and moving object detection using low rank approximation," *Future Generation Computer Systems*, vol. 90, pp. 198–210, 2019.
- [9] J. Peng, Y. Wang, H. Zhang, J. Wang, and D. Meng, "Exact decomposition of joint low rankness and local smoothness plus sparse matrices," *IEEE Transactions on Pattern Analysis and Machine Intelligence*, vol. 45, no. 5, pp. 5766–5781, 2022.
- [10] Z. Jia, Q. Jin, M. Ng, and X. Zhao, "Non-local robust quaternion matrix completion for large-scale color image and video inpainting," *IEEE Transactions on Image Processing*, vol. 31, pp. 3868–3883, 2022.
- [11] J. Zhao, "A novel low-rank matrix approximation algorithm for face denoising and background/foreground separation," *Computational and Applied Mathematics*, vol. 41, no. 4, pp. 165–203, 2022.
- [12] H. Yong, D. Meng, W. Zuo, and L. Zhang, "Robust online matrix factorization for dynamic background subtraction," *IEEE Transactions on Pattern Analysis and Machine Intelligence*, vol. 40, no. 7, pp. 1726–1740, 2017.
- [13] B. Recht, M. Fazel, and P. Parrilo, "Guaranteed minimum-rank solutions of linear matrix equations via nuclear norm minimization," *SIAM review*, vol. 52, no. 3, pp. 471–501, 2010.
- [14] M. Yang, Y. Li, and J. Wang, "Feature and nuclear norm minimization for matrix completion," *IEEE Transactions on Knowledge and Data Engineering*, vol. 34, no. 5, pp. 2190–2199, 2020.
- [15] X. Li, H. Zhang, and R. Zhang, "Matrix completion via non-convex relaxation and adaptive correlation learning," *IEEE Transactions on Pattern Analysis and Machine Intelligence*, vol. 45, no. 2, pp. 1981–1991, 2022.
- [16] E. Candès and B. Recht, "Exact matrix completion via convex optimization," *Communications of the ACM*, vol. 55, no. 6, pp. 111–119, 2012.
- [17] E. Candès and T. Tao, "The power of convex relaxation: Near-optimal matrix completion," *IEEE Transactions on Information Theory*, vol. 56, no. 5, pp. 2053–2080, 2010.
- [18] Q. Sun, S. Xiang, and J. Ye, "Robust principal component analysis via capped norms," in *Proceedings of the 19th ACM SIGKDD international conference on Knowledge discovery and data mining*, 2013, pp. 311–319.
- [19] F. Nie, H. Huang, and C. Ding, "Low-rank matrix recovery via efficient Schatten  $p$  norm minimization," in *Proceedings of the AAAI Conference on Artificial Intelligence*, vol. 26, no. 1, 2012, pp. 655–661.
- [20] S. Gu, L. Zhang, W. Zuo, and X. Feng, "Weighted nuclear norm minimization with application to image denoising," in *Proceedings of the IEEE conference on computer vision and pattern recognition*, 2014, pp. 2862–2869.
- [21] S. Gu, Q. Xie, D. Meng, W. Zuo, X. Feng, and L. Zhang, "Weighted nuclear norm minimization and its applications to low level vision," *International journal of computer vision*, vol. 121, pp. 183–208, 2017.
- [22] G. Li, G. Guo, S. Peng, C. Wang, S. Yu, J. Niu, and J. Mo, "Matrix completion via Schatten capped  $p$  norm," *IEEE Transactions on Knowledge and Data Engineering*, vol. 34, no. 1, pp. 394–404, 2020.
- [23] Z. Tan and H. Yang, "Total variation regularized multi-matrices weighted Schatten  $p$ -norm minimization for image denoising," *Applied Mathematical Modelling*, vol. 124, pp. 518–531, 2023.
- [24] S. Wang, K. Xia, L. Wang, Z. Yin, Z. He, J. Zhang, and N. Aslam, "Low-rank matrix factorization with nonconvex regularization and bilinear decomposition," *Signal Processing*, vol. 201, p. 108694, 2022.
- [25] Y. Xie, S. Gu, Y. Liu, W. Zuo, W. Zhang, and L. Zhang, "Weighted Schatten  $p$ -norm minimization for image denoising and background subtraction," *IEEE Transactions on Image Processing*, vol. 25, no. 10, pp. 4842–4857, 2016.

- [26] Q. Zhao, Y. Lin, F. Wang, and D. Meng, "Adaptive weighting function for weighted nuclear norm based matrix/tensor completion," *International Journal of Machine Learning and Cybernetics*, vol. 15, no. 2, pp. 697–718, 2024.
- [27] K. Gao, Z. Huang, and L. Guo, "Low-rank matrix recovery problem minimizing a new ratio of two norms approximating the rank function then using an admm-type solver with applications," *Journal of Computational and Applied Mathematics*, vol. 438, p. 115564, 2024.
- [28] E. Candès, X. Li, Y. Ma, and J. Wright, "Robust principal component analysis?" *Journal of the ACM*, vol. 58, no. 3, pp. 1–37, 2011.
- [29] J. Lin, T. Huang, X. Zhao, T. Ji, and Q. Zhao, "Tensor robust kernel pca for multidimensional data," *IEEE Transactions on Neural Networks and Learning Systems*, pp. 1–13, 2024.
- [30] J. Wright, A. Ganesh, S. Rao, Y. Peng, and Y. Ma, "Robust principal component analysis: Exact recovery of corrupted low-rank matrices via convex optimization," *Advances in neural information processing systems*, vol. 22, pp. 2080–2088, 2009.
- [31] G. Liu, Z. Lin, S. Yan, J. Sun, Y. Yu, and Y. Ma, "Robust recovery of subspace structures by low-rank representation," *IEEE Transactions on Pattern Analysis and Machine Intelligence*, vol. 35, no. 1, pp. 171–184, 2012.
- [32] Z. Zhou, X. Li, J. Wright, E. Candès, and Y. Ma, "Stable principal component pursuit," in *2010 IEEE international symposium on information theory*. IEEE, 2010, pp. 1518–1522.
- [33] R. Chartrand, "Nonconvex splitting for regularized low-rank + sparse decomposition," *IEEE Transactions on Signal Processing*, vol. 60, no. 11, pp. 5810–5819, 2012.
- [34] J. Wang, G. Xu, C. Li, Z. Wang, and F. Yan, "Surface defects detection using non-convex total variation regularized rpca with kernelization," *IEEE Transactions on Instrumentation and Measurement*, vol. 70, pp. 1–13, 2021.
- [35] L. Li, Z. Wang, Q. Hu, and Y. Dong, "Adaptive non-convex sparsity based background subtraction for intelligent video surveillance," *IEEE Transactions on Industrial Informatics*, vol. 17, no. 6, pp. 4168–4178, 2020.
- [36] P. Pokala, R. Hemadri, and C. Seelamantula, "Iteratively reweighted minimax-concave penalty minimization for accurate low-rank plus sparse matrix decomposition," *IEEE Transactions on Pattern Analysis and Machine Intelligence*, vol. 44, no. 12, pp. 8992–9010, 2021.
- [37] G. Yuan and B. Ghanem, "l<sub>0</sub> tv: A sparse optimization method for impulse noise image restoration," *IEEE Transactions on Pattern Analysis and Machine Intelligence*, vol. 41, no. 2, p. 352–364, 2019.
- [38] E. Wei and A. Ozdaglar, "Distributed alternating direction method of multipliers," in *2012 IEEE 51st IEEE Conference on Decision and Control*, 2012, pp. 5445–5450.
- [39] S. Boyd, N. Parikh, E. Chu, B. Peleato, and J. Eckstein, "Distributed optimization and statistical learning via the alternating direction method of multipliers," *Foundations and Trends in Machine Learning*, vol. 3, no. 1, pp. 1–122, 2011.
- [40] W. Lu, Z. Fang, L. Wu, L. Tang, and H. Liu, "A coupled non-convex hybrid regularization and weak  $H^{-1}$  image decomposition model for denoising application," *Journal of Applied Mathematics and Computing*, vol. 70, no. 1, pp. 197–233, 2024.
- [41] D. Hunter and K. Lange, "A tutorial on mm algorithms," *The American Statistician*, vol. 58, no. 1, pp. 30–37, 2004.
- [42] L. Wu, L. Tang, and C. Li, "Hybrid regularization model combining overlapping group sparse second-order total variation and nonconvex total variation," *Journal of Electronic Imaging*, vol. 31, no. 4, p. 043012, 2022.
- [43] H. Zhang, B. Yalcin, J. Lavaei, and S. Sojoudi, "A new complexity metric for nonconvex rank-one generalized matrix completion," *Mathematical Programming*, pp. 1–42, 2023.
- [44] L. Zhang, Y. Zhao, Z. Zhu, D. Shen, and S. Ji, "Multi-view missing data completion," *IEEE Transactions on Knowledge and Data Engineering*, vol. 30, no. 7, pp. 1296–1309, 2018.
- [45] E. J. Candès and B. Recht, "Multi-view missing data completion," *Foundations of Computational Mathematics*, vol. 9, no. 6, pp. 717–772, 2009.
- [46] Y. Sun, P. Babu, and D. Palomar, "Majorization-minimization algorithms in signal processing, communications, and machine learning," *IEEE Transactions on Signal Processing*, vol. 65, no. 3, pp. 794–816, 2016.
- [47] R. Vershynin, "High-dimensional probability: An introduction with applications in data science," *University of California, Irvine*, 2024.
- [48] H. Zhang, F. Qian, P. Shi, W. Du, Y. Tang, J. Qian, C. Gong, and J. Yang, "Generalized nonconvex nonsmooth low-rank matrix recovery framework with feasible algorithm designs and convergence analysis," *IEEE Transactions on Neural Networks and Learning Systems*, vol. 34, no. 9, pp. 5342–5353, 2023.
- [49] L. Mirsky, "A trace inequality of john von neumann," *Monatshefte für Mathematik*, vol. 79, no. 4, pp. 303–306, 1975.
- [50] J. Yang and X. Yuan, "Linearized augmented lagrangian and alternating direction methods for nuclear norm minimization," *Mathematics of computation*, vol. 82, no. 281, pp. 301–329, 2013.
- [51] X. Zhang, D. Peng, and Y. Su, "A singular value shrinkage thresholding algorithm for folded concave penalized low-rank matrix optimization problems," *Journal of Global Optimization*, vol. 88, no. 2, pp. 485–508, 2024.
- [52] H. Zhang, B. Wen, Z. Zha, B. Zhang, Y. Tang, G. Yu, and W. Du, "Accelerated palm for nonconvex low-rank matrix recovery with theoretical analysis," *IEEE Transactions on Circuits and Systems for Video Technology*, vol. 34, no. 4, pp. 2304–2317, 2024.
- [53] Y. Jiao, Q. Jin, X. Lu, and W. Wang, "Alternating direction method of multipliers for linear inverse problems," *SIAM Journal on Numerical Analysis*, vol. 54, no. 4, pp. 2114–2137, 2016.



**Wenjing Lu** was born in 2000. She is currently pursuing her M.S. at Hubei Minzu University. Her main research interests are data analysis and image processing.



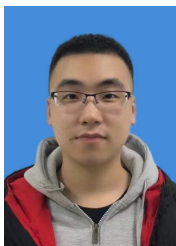
**Zhuang Fang** was born in 1980. He received the B.S degree from Hubei Minzu University in 2003 and the M.S. degree from Chongqing University in 2011, and Ph.D. degree from Wuhan University in 2019. He is currently an associate professor in the School of Mathematics and Statistics at Hubei Minzu University. His research focuses on image processing, mathematical modeling and low-rank matrix recovery.



**Liang Wu** was born in 1998. He received the M.S. degree from Hubei Minzu University in 2020. He is currently pursuing a Ph.D. degree with the School of Mathematics and Statistics, Southwest University, Chongqing, China. His current research interests include image processing, low-rank matrix/tensor analysis and high dimensional data modeling.



**Liming Tang** was born in 1978. He received the B.S. degree from Hubei Minzu University in 2000, the M.S. degree from Chongqing University in 2007, and Ph.D. degree in computational mathematics from Chongqing University in 2013. He is currently a professor in the School of Mathematics and Statistics at Hubei Minzu University. His research interests include image processing, computer vision and pattern recognition.



**Hanxin Liu** was born in 1997. He is currently pursuing his M.S. at Hubei Minzu University. His main research interests are noise estimation and image processing.

APPENDIX A  
PROOF OF THEOREM 1

*Proof.* The matrix  $\mathbf{M}$  can be decomposed into  $\mathbf{M} = \mathbf{U}\mathbf{\Sigma}\mathbf{V}^T$ , where  $\mathbf{U}$  and  $\mathbf{V}$  are orthogonal matrices,  $\mathbf{\Sigma}$  is a diagonal matrix with diagonal elements  $\sigma_i$  and  $r = \min\{n_1, n_2\}$  is the rank of  $\mathbf{M}$ .

Since the matrix  $\mathbf{M}_k$  preserves the first  $k$  non-zero singular values in  $\mathbf{\Sigma}$ , we have  $\mathbf{M}_k = \mathbf{U}\mathbf{\Sigma}_k\mathbf{V}^T$ , where  $\mathbf{\Sigma}_k = \text{diag}(\sigma_1, \sigma_2, \dots, \sigma_k, 0, \dots, 0)$ .

To simplify the calculation, we express the Frobenius norm of the error matrix  $\|\mathbf{M} - \mathbf{M}_k\|_F^2$  as follows,

$$\|\mathbf{M} - \mathbf{M}_k\|_F^2 = \text{tr}\left((\mathbf{M} - \mathbf{M}_k)^T(\mathbf{M} - \mathbf{M}_k)\right). \quad (35)$$

The error matrix  $(\mathbf{M} - \mathbf{M}_k)$  can be expanded into the singular value form, that is

$$\mathbf{M} - \mathbf{M}_k = \sum_{i=k+1}^r \sigma_i u_i v_i^T, \quad (36)$$

where  $u_i$  and  $v_i$  are the  $i$ -th left and right singular vectors of  $\mathbf{M}$ , respectively.

According to the trace operation formula, Eq. (35) can be written as

$$\begin{aligned} \|\mathbf{M} - \mathbf{M}_k\|_F^2 &= \text{tr}\left(\left(\sum_{i=k+1}^r \sigma_i u_i v_i^T\right)^T \left(\sum_{i=k+1}^r \sigma_i u_i v_i^T\right)\right) \\ &= \text{tr}\left(\left(\sum_{i=k+1}^r \sigma_i v_i u_i^T\right)^T \left(\sum_{i=k+1}^r \sigma_i u_i v_i^T\right)\right) \\ &= \text{tr}\left(\sum_{i=k+1}^r \sigma_i v_i u_i^T\right) \\ &= \sum_{i=k+1}^r \sigma_i^2 \text{tr}(v_i v_i^T). \end{aligned} \quad (37)$$

Therefore, we can obtain

$$\|\mathbf{M} - \mathbf{M}_k\|_F^2 = \sum_{i=k+1}^r \sigma_i^2. \quad (38)$$

Then,  $\|\mathbf{M} - \mathbf{M}_k\|_F^2$  can be expressed by the singular value  $\sigma_i$  of  $\mathbf{M}$ .

Thus, Theorem 2 is obtained.  $\square$

APPENDIX B  
PROOF OF THEOREM 2

*Proof.* To prove Theorem 3, we first define some terms. Given two matrices  $\mathcal{E}_1 \in \mathbb{R}^{n_1 \times n_2}$  and  $\mathcal{E}_2 \in \mathbb{R}^{n_1 \times n_2}$ , where  $\mathcal{E}_{1(i,j),K}$  and  $\mathcal{E}_{2(i,j),K}$  represent points groups of size  $K * K$  centered on  $(i, j)$ .

According to the definition of convex function, we need to prove that for any  $\mathcal{E}_1, \mathcal{E}_2$ , and  $\theta \in [0, 1]$ , it holds that

$$\phi(\theta\mathcal{E}_1 + (1 - \theta)\mathcal{E}_2) \leq \theta\phi(\mathcal{E}_1) + (1 - \theta)\phi(\mathcal{E}_2). \quad (39)$$

Then the function  $\phi(\mathcal{E})$  is a convex function.

By the definition of  $\phi(\mathcal{E})$ , we expand the term  $\phi(\theta\mathcal{E}_1 + (1 - \theta)\mathcal{E}_2)$  on the left side of inequality (39), for each  $(i, j)$ , we have

$$\sum_{i,j=1}^{n_2} \left[ \sum_{k_1, k_2=-n_1}^{n_2} |\theta\varepsilon_1(i+k_1, j+k_2) + (1-\theta)\varepsilon_2(i+k_1, j+k_2)|^2 \right]^{\frac{1}{2}}, \quad (40)$$

where  $\varepsilon_1$  and  $\varepsilon_2$  are elements of  $\mathcal{E}_1$  and  $\mathcal{E}_2$ , respectively.

By the property of absolute value inequality, for any  $a, b, \theta \in \mathbb{R}$ , there is

$$|\theta a + (1 - \theta)b| \leq \theta|a| + (1 - \theta)|b|. \quad (41)$$

Applying this property to inequality (39), we have

$$\begin{aligned} &|\theta\varepsilon_1(i+k_1, j+k_2) + (1-\theta)\varepsilon_2(i+k_1, j+k_2)| \\ &\leq \theta|\varepsilon_1(i+k_1, j+k_2)| + (1-\theta)|\varepsilon_2(i+k_1, j+k_2)|. \end{aligned} \quad (42)$$

Since the square function is convex, we square both sides of the inequality, that is

$$\begin{aligned} &(\theta\varepsilon_1(i+k_1, j+k_2) + (1-\theta)\varepsilon_2(i+k_1, j+k_2))^2 \\ &\leq \theta|\varepsilon_1(i+k_1, j+k_2)|^2 + (1-\theta)|\varepsilon_2(i+k_1, j+k_2)|^2. \end{aligned} \quad (43)$$

By summing up the above inequality for all  $i, j, k_1, k_2$ , we get

$$\phi(\theta\mathcal{E}_1 + (1 - \theta)\mathcal{E}_2) \leq \theta\phi(\mathcal{E}_1) + (1 - \theta)\phi(\mathcal{E}_2). \quad (44)$$

By the definition of convex functions, we have proved that  $\phi(\mathcal{E})$  is a convex function.

Thus, Theorem 3 is obtained.  $\square$

APPENDIX C  
PROOF OF THEOREM 3

*Proof.* The matrices  $\mathbf{W}$  and  $\mathbf{D}$  are subjected to singular value decomposition to obtain  $\mathbf{W} = \mathbf{U}_W \mathbf{\Sigma}_W \mathbf{V}_W^T$  and  $\mathbf{D} = \mathbf{Q}_D \mathbf{S}_D \mathbf{R}_D^T$ , where  $\mathbf{\Sigma}_W$  and  $\mathbf{S}_D$  are the diagonal matrices of  $\mathbf{W}$  and  $\mathbf{D}$ , respectively. Consequently, problem (15) can be rewritten as

$$\lambda \sum_{i=1}^{\min\{n_1, n_2\}} \psi(\sigma_i) + \frac{\rho}{2} \|\mathbf{U}_W \mathbf{\Sigma}_W \mathbf{V}_W^T - \mathbf{Q}_D \mathbf{S}_D \mathbf{R}_D^T\|_F^2. \quad (45)$$

According to Lemma 1, it follows that

$$\begin{aligned} &\|\mathbf{U}_W \mathbf{\Sigma}_W \mathbf{V}_W^T - \mathbf{Q}_D \mathbf{S}_D \mathbf{R}_D^T\|_F^2 \\ &= \text{tr}(\mathbf{\Sigma}_W^T \mathbf{\Sigma}_W) + \text{tr}(\mathbf{S}_D^T \mathbf{S}_D) - 2\text{tr}(\mathbf{W}^T \mathbf{D}) \\ &\geq \text{tr}(\mathbf{\Sigma}_W^T \mathbf{\Sigma}_W) + \text{tr}(\mathbf{S}_D^T \mathbf{S}_D) - 2\text{tr}(\mathbf{\Sigma}_W^T \mathbf{S}_D) \\ &= \|\mathbf{\Sigma}_W^T \mathbf{S}_D\|_F^2 \\ &= \sum_{i=1}^{\min\{n_1, n_2\}} (\sigma_i - s_i)^2, \end{aligned} \quad (46)$$

where the equation in the above formula holds if and only if  $\mathbf{U}_W = \mathbf{Q}_D, \mathbf{V}_W = \mathbf{R}_D$ .

Therefore, the optimal numerical solution of problem (45) can be written as

$$\min_{\sigma_i} \lambda \sum_{i=1}^{\min\{n_1, n_2\}} \psi(\sigma_i) + \frac{\rho}{2} \sum_{i=1}^{\min\{n_1, n_2\}} (\sigma_i - s_i)^2. \quad (47)$$

Simplification of the above equation yields that

$$\min_{\sigma_i} \lambda \psi(\sigma_i) + \frac{\rho}{2} (\sigma_i - s_i)^2. \quad (48)$$

Thus, Theorem 4 is obtained.  $\square$

APPENDIX D  
SOLVE THE E-SUBPROBLEM

The  $\mathbf{E}$ -subproblem (22) is expressed as

$$\mathbf{E}^{k+1} = \arg \min_{\mathbf{E}} \lambda \phi(\mathbf{E}) + \frac{\rho}{2} \left\| \mathbf{E} - \mathcal{E}^{k+1} + \frac{\boldsymbol{\mu}_2^k}{\rho} \right\|_F^2. \quad (49)$$

For convenience, we reformulate the above equation as

$$\mathbf{E}^{k+1} = \arg \min_{\mathbf{E}} \left\{ J(\mathbf{E}) = \lambda \phi(\mathbf{E}) + \frac{\rho}{2} \|\mathbf{E} - \mathbf{D}^k\|_F^2 \right\}, \quad (50)$$

where  $\mathbf{D}^k = \mathcal{E}^{k+1} + \frac{\mu_2^k}{\rho}$ . It can be seen from the mean inequality that, for all  $\forall \mathbf{V} \in R^{\dim(\mathbf{E})}$ , we have the following,

$$\begin{aligned} \phi(\mathbf{E}) &= \sum_{i,j=1} \|\mathbf{E}_{(i,j),K}\|_2 \\ &\leq \sum_{i,j=1} \left( \frac{\|\mathbf{E}_{(i,j),K}\|_2^2}{2\|\mathbf{V}_{(i,j),K}\|_2} + \frac{1}{2}\|\mathbf{V}_{(i,j),K}\|_2 \right) \\ &= S(\mathbf{E}, \mathbf{V}). \end{aligned} \quad (51)$$

Thus, we claim that  $T(\mathbf{E}, \mathbf{V}) = \lambda S(\mathbf{E}, \mathbf{V}) + \frac{\rho}{2}\|\mathbf{E} - \mathbf{D}^k\|_F^2$  is a substitute function of the function  $\phi(\mathbf{E})$  at point  $\mathbf{V}$ . In addition, there are two facts here: (i)  $T(\mathbf{E}, \mathbf{V}) \geq J(\mathbf{E})$  and (ii)  $T(\mathbf{V}, \mathbf{V}) = J(\mathbf{V})$ . Furthermore, by Theorem 1, we may as well take  $\mathbf{V} = \mathbf{E}^k$  and convert the  $\mathbf{E}$ -subproblem into

$$\begin{aligned} \mathbf{E}^{k+1} &= \arg \min_{\mathbf{E}} T(\mathbf{E}, \mathbf{E}^k) \\ &= \arg \min_{\mathbf{E}} \frac{\rho}{2}\|\mathbf{E} - \mathbf{D}^k\|_F^2 + \frac{\lambda}{2}\|\mathbf{\Lambda}(\mathbf{E}^k)\mathbf{E}\|_2^2 + \mathbf{C}, \end{aligned} \quad (52)$$

where  $\mathbf{C}$  is a constant independent of the variable  $\mathbf{E}$  and  $\mathbf{\Lambda}(\mathbf{E}^k)$  is a diagonal matrix whose elements on the diagonal can be expressed as

$$[\mathbf{\Lambda}(\mathbf{E}^k)]_{l,l} = \sqrt{\sum_{i,j=-m_1}^{m_2} \left[ \sum_{k_1, k_2=-m_1}^{m_2} |\mathbf{E}^k_{r-i+k_1, i-j+k_2}|^2 \right]^{-1/2}}.$$

Finally, we find the optimized solution of the  $\mathbf{E}$ -subproblem as

$$\mathbf{E}^{k+1} = \left( \mathbf{I} + \frac{\lambda \mathbf{\Lambda}(\mathbf{E}^k)^T \mathbf{\Lambda}(\mathbf{E}^k)}{\rho} \right)^{-1} \mathbf{D}^k. \quad (53)$$

#### APPENDIX E PROOF OF THEOREM 4

*Proof.* Firstly, we prove that the function  $L$  is strictly convex with respect to the  $\mathbf{X}$ -subproblem.

Expanding the first term of Eq. (10), we have

$$\begin{aligned} \left\| \mathbf{W} - \mathbf{X} + \frac{\mu_1}{\rho} \right\|_F^2 &= \|\mathbf{X}\|_F^2 + \left\langle \mathbf{X}, -\mathbf{W} - \frac{\mu_1}{\rho} \right\rangle \\ &+ \left\| -\mathbf{W} - \frac{\mu_1}{\rho} \right\|_F^2. \end{aligned} \quad (54)$$

Considering that this term is a linear term with respect to  $\mathbf{X}$ , i.e., it is convex.

Next, expanding the second term of Eq. (10), we get

$$\begin{aligned} &\left\| \mathbf{F}_\Omega - (\mathbf{Y}_\Omega - \mathbf{X}_\Omega - \mathcal{E}_\Omega) + \frac{\mu_3}{\rho} \right\|_F^2 \\ &= \|\mathbf{X}\|_F^2 + \left\langle \mathbf{X}, \mathbf{F}_\Omega - (\mathbf{Y}_\Omega - \mathcal{E}_\Omega) + \frac{\mu_3}{\rho} \right\rangle \\ &+ \left\| \mathbf{F}_\Omega - (\mathbf{Y}_\Omega - \mathcal{E}_\Omega) + \frac{\mu_3}{\rho} \right\|_F^2 \end{aligned} \quad (55)$$

It can be seen that this term is also a linear term with respect to  $\mathbf{X}$ , meaning it is also convex.

Therefore, it is demonstrated that the function  $L$  is strictly convex with respect to the  $\mathbf{X}$ -subproblem.

The Taylor expansion and the properties of convex functions [50] indicate that

$$f(\mathbf{X}^{k+1}) \geq f(\mathbf{X}^k) + \langle \nabla f(\mathbf{X}^k), \mathbf{X}^{k+1} - \mathbf{X}^k \rangle. \quad (56)$$

Consequently, we can deduce that there must exist positive constants  $c_1$  and  $c_2$  such that the following inequality holds,

$$\begin{aligned} &L(\mathbf{X}^{k+1}, \mathbf{W}^k, \mathcal{E}^k, \mathbf{F}_\Omega^k, \mathbf{E}^k, \mu_1^k, \mu_2^k, \mu_3^k) \\ &- L(\mathbf{X}^k, \mathbf{W}^k, \mathcal{E}^k, \mathbf{F}_\Omega^k, \mathbf{E}^k, \mu_1^k, \mu_2^k, \mu_3^k) \\ &\leq -c_1 \|\mathbf{X}^{k+1} - \mathbf{X}^k\|_F^2 - c_2 \|\mathbf{X}_\Omega^{k+1} - \mathbf{X}_\Omega^k\|_F^2 \\ &+ \langle \nabla_{\mathbf{X}} L(\mathbf{X}^{k+1}), \mathbf{X}^{k+1} - \mathbf{X}^k \rangle, \end{aligned} \quad (57)$$

where  $\mathbf{I}(\mathbf{X}^{k+1}) = L(\mathbf{X}^{k+1}, \mathbf{W}^k, \mathcal{E}^k, \mathbf{F}_\Omega^k, \mathbf{E}^k, \mu_1^k, \mu_2^k, \mu_3^k)$  represents the gradient of the function  $L$  with respect to  $\mathbf{X}$  at point  $\mathbf{X}^{k+1}$ . Since  $\mathbf{X}^{k+1}$  is the point at which  $L$  reaches a local minimum, we have

$$\nabla_{\mathbf{X}} L(\mathbf{X}^{k+1}, \mathbf{W}^k, \mathcal{E}^k, \mathbf{F}_\Omega^k, \mathbf{E}^k, \mu_1^k, \mu_2^k, \mu_3^k) = 0. \quad (58)$$

Combining (57) and (58), we can obtain

$$\begin{aligned} &L(\mathbf{X}^{k+1}, \mathbf{W}^k, \mathcal{E}^k, \mathbf{F}_\Omega^k, \mathbf{E}^k, \mu_1^k, \mu_2^k, \mu_3^k) \\ &- L(\mathbf{X}^k, \mathbf{W}^k, \mathcal{E}^k, \mathbf{F}_\Omega^k, \mathbf{E}^k, \mu_1^k, \mu_2^k, \mu_3^k) \\ &\leq -c_1 \|\mathbf{X}^{k+1} - \mathbf{X}^k\|_F^2 - c_2 \|\mathbf{X}_\Omega^{k+1} - \mathbf{X}_\Omega^k\|_F^2. \end{aligned} \quad (59)$$

Thus, Theorem 5 is obtained.  $\square$

#### APPENDIX F PROOF OF THEOREM 5

*Proof.* Considering that  $R(\mathbf{W})$  is a generalized approximation function of a rank function, it is necessary to discuss it separately as a convex and non-convex approximation function.

(i) If  $R(\mathbf{W})$  is a convex approximation function, we can determine from (13) that function  $L$  is strictly convex with respect to the  $\mathbf{W}$ -subproblem.

Similar to Theorem 5, we can deduce that there must exist a positive constant  $c_3$  such that the following inequality holds,

$$\begin{aligned} &L(\mathbf{X}^{k+1}, \mathbf{W}^{k+1}, \mathcal{E}^k, \mathbf{F}_\Omega^k, \mathbf{E}^k, \mu_1^k, \mu_2^k, \mu_3^k) \\ &- L(\mathbf{X}^{k+1}, \mathbf{W}^k, \mathcal{E}^k, \mathbf{F}_\Omega^k, \mathbf{E}^k, \mu_1^k, \mu_2^k, \mu_3^k) \\ &\leq -\alpha c_3 \|\mathbf{W}^{k+1} - \mathbf{W}^k\|_F^2. \end{aligned} \quad (60)$$

(ii) If  $R(\mathbf{W})$  is a non-convex approximation function, then since  $\mathbf{W}^{k+1}$  is a minimum in the minimization problem (13), we have

$$\begin{aligned} &\alpha \langle \nabla R(\mathbf{W}^k), \mathbf{W}^{k+1} - \mathbf{W}^k \rangle \\ &+ \frac{\rho}{2} \left\| \mathbf{W}^{k+1} - \mathbf{X}^{k+1} + \frac{\mu_1^k}{\rho} \right\|_F^2 \\ &\leq \frac{\rho}{2} \left\| \mathbf{W}^k - \mathbf{X}^{k+1} + \frac{\mu_1^k}{\rho} \right\|_F^2. \end{aligned} \quad (61)$$

It follows from Assumption 1 and the properties of non-convex functions [51], [52] that there must exist a positive constant  $c_3$  such that

$$\begin{aligned} R(\mathbf{W}^{k+1}) &\leq R(\mathbf{W}^k) + \langle \nabla R(\mathbf{W}^k), \mathbf{W}^{k+1} - \mathbf{W}^k \rangle \\ &- c_3 \|\mathbf{W}^{k+1} - \mathbf{W}^k\|_F^2. \end{aligned} \quad (62)$$

Combining (61) and (62), we obtain

$$\begin{aligned} &\alpha R(\mathbf{W}^{k+1}) + \frac{\rho}{2} \left\| \mathbf{W}^{k+1} - \mathbf{X}^{k+1} + \frac{\mu_1^k}{\rho} \right\|_F^2 \\ &\leq \alpha R(\mathbf{W}^k) + \frac{\rho}{2} \left\| \mathbf{W}^k - \mathbf{X}^{k+1} + \frac{\mu_1^k}{\rho} \right\|_F^2. \end{aligned} \quad (63)$$

This implies that

$$\begin{aligned} & L(\mathbf{X}^{k+1}, \mathbf{W}^{k+1}, \mathcal{E}^k, \mathbf{F}_\Omega^k, \mathbf{E}^k, \boldsymbol{\mu}_1^k, \boldsymbol{\mu}_2^k, \boldsymbol{\mu}_3^k) \\ & - L(\mathbf{X}^{k+1}, \mathbf{W}^k, \mathcal{E}^k, \mathbf{F}_\Omega^k, \mathbf{E}^k, \boldsymbol{\mu}_1^k, \boldsymbol{\mu}_2^k, \boldsymbol{\mu}_3^k) \\ & \leq -\alpha c_3 \|\mathbf{W}^{k+1} - \mathbf{W}^k\|_F^2. \end{aligned} \quad (64)$$

By (i) and (ii), Theorem 6 is obtained.  $\square$

#### APPENDIX G PROOF OF THEOREM 6

*Proof.* (i) We can determine from (17) that function  $L$  is strictly convex with respect to the  $\mathcal{E}$ -subproblem.

Similar to Theorem 5, we can deduce that there must exist positive constants  $c_4$  and  $c_5$  such that the following inequality holds,

$$\begin{aligned} & L(\mathbf{X}^{k+1}, \mathbf{W}^{k+1}, \mathcal{E}^{k+1}, \mathbf{F}_\Omega^k, \mathbf{E}^k, \boldsymbol{\mu}_1^k, \boldsymbol{\mu}_2^k, \boldsymbol{\mu}_3^k) \\ & - L(\mathbf{X}^{k+1}, \mathbf{W}^{k+1}, \mathcal{E}^k, \mathbf{F}_\Omega^k, \mathbf{E}^k, \boldsymbol{\mu}_1^k, \boldsymbol{\mu}_2^k, \boldsymbol{\mu}_3^k) \\ & \leq -c_4 \|\mathcal{E}^{k+1} - \mathcal{E}^k\|_F^2 - c_5 \|\mathcal{E}_\Omega^{k+1} - \mathcal{E}_\Omega^k\|_F^2. \end{aligned} \quad (65)$$

(ii) Similarly, we can determine from (20) that function  $L$  is strictly convex with respect to the  $\mathbf{F}_\Omega$ -subproblem.

Therefore, we can deduce that there exists a positive constant  $c_6$  such that the following inequality holds,

$$\begin{aligned} & L(\mathbf{X}^{k+1}, \mathbf{W}^{k+1}, \mathcal{E}^{k+1}, \mathbf{F}_\Omega^{k+1}, \mathbf{E}^k, \boldsymbol{\mu}_1^k, \boldsymbol{\mu}_2^k, \boldsymbol{\mu}_3^k) \\ & - L(\mathbf{X}^{k+1}, \mathbf{W}^{k+1}, \mathcal{E}^{k+1}, \mathbf{F}_\Omega^k, \mathbf{E}^k, \boldsymbol{\mu}_1^k, \boldsymbol{\mu}_2^k, \boldsymbol{\mu}_3^k) \\ & \leq -c_6 \|\mathbf{F}_\Omega^{k+1} - \mathbf{F}_\Omega^k\|_F^2 \end{aligned} \quad (66)$$

(iii) Considering that we have proved that  $\phi(\cdot)$  is a convex function in Theorem 3.

Similarly, we can determine from (22) that function  $L$  is strictly convex with respect to the  $\mathbf{E}$ -subproblem.

Therefore, we can deduce that there exists a positive constant  $c_7$  such that the following inequality holds,

$$\begin{aligned} & L(\mathbf{X}^{k+1}, \mathbf{W}^{k+1}, \mathcal{E}^{k+1}, \mathbf{F}_\Omega^{k+1}, \mathbf{E}^{k+1}, \boldsymbol{\mu}_1^k, \boldsymbol{\mu}_2^k, \boldsymbol{\mu}_3^k) \\ & - L(\mathbf{X}^{k+1}, \mathbf{W}^{k+1}, \mathcal{E}^{k+1}, \mathbf{F}_\Omega^{k+1}, \mathbf{E}^k, \boldsymbol{\mu}_1^k, \boldsymbol{\mu}_2^k, \boldsymbol{\mu}_3^k) \\ & \leq -\lambda c_7 \|\mathbf{E}^{k+1} - \mathbf{E}^k\|_F^2. \end{aligned} \quad (67)$$

Based on (i), (ii) and (iii), Theorem 7 is obtained.  $\square$

#### APPENDIX H PROOF OF THEOREM 7

*Proof.* Considering that  $\mathbf{W}^{k+1}$ ,  $\mathbf{F}_\Omega^{k+1}$ , and  $\mathbf{E}^{k+1}$  are minima in the minimization problems (13), (20), and (22), respectively, we have

$$\alpha \nabla R(\mathbf{W}^{k+1}) + \rho \left( \mathbf{W}^{k+1} - \mathbf{X}^{k+1} + \frac{\boldsymbol{\mu}_1^k}{\rho} \right) = 0, \quad (68)$$

$$\lambda \nabla \phi(\mathbf{E}^{k+1}) + \rho \left( \mathbf{E}^{k+1} - \mathcal{E}^{k+1} + \frac{\boldsymbol{\mu}_2^k}{\rho} \right) = 0, \quad (69)$$

$$\mathbf{F}_\Omega^{k+1} + \rho \left( \mathbf{F}_\Omega^{k+1} - (\mathbf{Y}_\Omega - \mathbf{X}_\Omega^{k+1} - \mathcal{E}_\Omega^{k+1}) + \frac{\boldsymbol{\mu}_3^k}{\rho} \right) = 0. \quad (70)$$

Combining (24) through (26), we obtain

$$\boldsymbol{\mu}_1^{k+1} + \alpha \nabla R(\mathbf{W}^{k+1}) = 0, \quad (71)$$

$$\boldsymbol{\mu}_2^{k+1} + \lambda \nabla \phi(\mathbf{E}^{k+1}) = 0, \quad (72)$$

$$\boldsymbol{\mu}_3^{k+1} + \mathbf{F}_\Omega^{k+1} = 0. \quad (73)$$

Further, by Assumption 1, we can deduce that there must exist positive constants  $c_8$ ,  $c_9$  and  $c_{10}$  such that the following inequality holds,

$$\begin{aligned} \|\boldsymbol{\mu}_1^{k+1} - \boldsymbol{\mu}_1^k\|_F^2 &= \|-\alpha \nabla R(\mathbf{W}^{k+1}) + \alpha \nabla R(\mathbf{W}^k)\|_F^2 \\ &\leq c_8 \|\mathbf{W}^{k+1} - \mathbf{W}^k\|_F^2, \end{aligned} \quad (74)$$

$$\begin{aligned} \|\boldsymbol{\mu}_2^{k+1} - \boldsymbol{\mu}_2^k\|_F^2 &= \|-\lambda \nabla \phi(\mathbf{E}^{k+1}) + \lambda \nabla \phi(\mathbf{E}^k)\|_F^2 \\ &\leq c_9 \|\mathbf{E}^{k+1} - \mathbf{E}^k\|_F^2, \end{aligned} \quad (75)$$

$$\begin{aligned} \|\boldsymbol{\mu}_3^{k+1} - \boldsymbol{\mu}_3^k\|_F^2 &= \|-\mathbf{F}_\Omega^{k+1} + \mathbf{F}_\Omega^k\|_F^2 \\ &\leq c_{10} \|\mathbf{F}_\Omega^{k+1} - \mathbf{F}_\Omega^k\|_F^2. \end{aligned} \quad (76)$$

where  $c_8 = \alpha^2 S_1^2$ ,  $c_9 = \lambda^2 S_2^2$ .

This implies that

$$\begin{aligned} & L(\mathbf{X}^{k+1}, \mathbf{W}^{k+1}, \mathcal{E}^{k+1}, \mathbf{F}_\Omega^{k+1}, \mathbf{E}^{k+1}, \boldsymbol{\mu}_1^{k+1}, \boldsymbol{\mu}_2^{k+1}, \boldsymbol{\mu}_3^{k+1}) \\ & - L(\mathbf{X}^{k+1}, \mathbf{W}^{k+1}, \mathcal{E}^{k+1}, \mathbf{F}_\Omega^{k+1}, \mathbf{E}^k, \boldsymbol{\mu}_1^k, \boldsymbol{\mu}_2^k, \boldsymbol{\mu}_3^k) \\ & = \langle \boldsymbol{\mu}_1^{k+1} - \boldsymbol{\mu}_1^k, \mathbf{W}^{k+1} - \mathbf{X}^{k+1} \rangle \\ & + \langle \boldsymbol{\mu}_2^{k+1} - \boldsymbol{\mu}_2^k, \mathbf{E}^{k+1} - \mathcal{E}^{k+1} \rangle \\ & + \langle \boldsymbol{\mu}_3^{k+1} - \boldsymbol{\mu}_3^k, \mathbf{F}_\Omega^{k+1} - \mathbf{Y}_\Omega + \mathbf{X}_\Omega^{k+1} + \mathcal{E}_\Omega^{k+1} \rangle \\ & \leq \frac{c_8}{\rho} \|\mathbf{W}^{k+1} - \mathbf{W}^k\|_F^2 + \frac{c_9}{\rho} \|\mathbf{E}^{k+1} - \mathbf{E}^k\|_F^2 \\ & + \frac{c_{10}}{\rho} \|\mathbf{F}_\Omega^{k+1} - \mathbf{F}_\Omega^k\|_F^2. \end{aligned} \quad (77)$$

Thus, Theorem 8 is obtained.  $\square$

#### APPENDIX I PROOF OF THEOREM 8

*Proof.* Through Theorems 5-8, the difference between two consecutive iterations of the function  $L$  in the iterative process of Algorithm 2 is described as follows,

$$\begin{aligned} & L(\mathbf{X}^{k+1}, \mathbf{W}^{k+1}, \mathcal{E}^{k+1}, \mathbf{F}_\Omega^{k+1}, \mathbf{E}^{k+1}, \boldsymbol{\mu}_1^{k+1}, \boldsymbol{\mu}_2^{k+1}, \boldsymbol{\mu}_3^{k+1}) \\ & - L(\mathbf{X}^k, \mathbf{W}^k, \mathcal{E}^k, \mathbf{F}_\Omega^k, \mathbf{E}^k, \boldsymbol{\mu}_1^k, \boldsymbol{\mu}_2^k, \boldsymbol{\mu}_3^k) \\ & = -c_1 \|\mathbf{X}^{k+1} - \mathbf{X}^k\|_F^2 - c_2 \|\mathbf{X}_\Omega^{k+1} - \mathbf{X}_\Omega^k\|_F^2 \\ & - (\alpha c_3 - c_8) \|\mathbf{W}^{k+1} - \mathbf{W}^k\|_F^2 - c_4 \|\mathcal{E}^{k+1} - \mathcal{E}^k\|_F^2 \\ & - c_5 \|\mathcal{E}_\Omega^{k+1} - \mathcal{E}_\Omega^k\|_F^2 - (c_6 - c_{10}) \|\mathbf{F}_\Omega^{k+1} - \mathbf{F}_\Omega^k\|_F^2 \\ & - (\lambda c_7 - c_9) \|\mathbf{E}^{k+1} - \mathbf{E}^k\|_F^2 \end{aligned} \quad (78)$$

Then, the following inequality holds when  $\rho \geq \max\left\{\frac{c_8}{\alpha c_3}, \frac{c_9}{\lambda c_7}, \frac{c_{10}}{c_6}\right\}$ ,

$$\begin{aligned} & L(\mathbf{X}^{k+1}, \mathbf{W}^{k+1}, \mathcal{E}^{k+1}, \mathbf{F}_\Omega^{k+1}, \mathbf{E}^{k+1}, \boldsymbol{\mu}_1^{k+1}, \boldsymbol{\mu}_2^{k+1}, \boldsymbol{\mu}_3^{k+1}) \\ & \leq L(\mathbf{X}^k, \mathbf{W}^k, \mathcal{E}^k, \mathbf{F}_\Omega^k, \mathbf{E}^k, \boldsymbol{\mu}_1^k, \boldsymbol{\mu}_2^k, \boldsymbol{\mu}_3^k). \end{aligned} \quad (79)$$

Thus, Theorem 9 is obtained.  $\square$

APPENDIX J  
PROOF OF THEOREM 9

*Proof.* According to (8), the function  $L$  can be written in the following form,

$$\begin{aligned}
L(\mathbf{X}^{k+1}, \mathbf{W}^{k+1}, \mathcal{E}^{k+1}, \mathbf{F}_\Omega^{k+1}, \mathbf{E}^{k+1}, \boldsymbol{\mu}_1^{k+1}, \boldsymbol{\mu}_2^{k+1}, \boldsymbol{\mu}_3^{k+1}) \\
&= \alpha R(\mathbf{W}^{k+1}) + \lambda \phi(\mathbf{E}^{k+1}) + \frac{1}{2} \|\mathbf{F}_\Omega^{k+1}\|_F^2 \\
&+ \frac{\rho}{2} \left\| \mathbf{W}^{k+1} - \mathbf{X}^{k+1} + \frac{\boldsymbol{\mu}_1^{k+1}}{\rho} \right\|_F^2 \\
&+ \frac{\rho}{2} \left\| \mathbf{E}^{k+1} - \mathcal{E}_\Omega^{k+1} + \frac{\boldsymbol{\mu}_2^{k+1}}{\rho} \right\|_F^2 \\
&+ \frac{\rho}{2} \left\| \mathbf{F}_\Omega^{k+1} - (\mathbf{Y}_\Omega - \mathbf{X}_\Omega^{k+1} - \mathcal{E}_\Omega^{k+1}) + \frac{\boldsymbol{\mu}_3^{k+1}}{\rho} \right\|_F^2 \\
&\geq \alpha R(\mathbf{W}^{k+1}) + \lambda \phi(\mathbf{E}^{k+1}) \\
&+ \frac{\rho}{2} \left\| \mathbf{W}^{k+1} - \mathbf{X}^{k+1} + \frac{\boldsymbol{\mu}_1^{k+1}}{\rho} \right\|_F^2 \\
&+ \frac{\rho}{2} \left\| \mathbf{E}^{k+1} - \mathcal{E}_\Omega^{k+1} + \frac{\boldsymbol{\mu}_2^{k+1}}{\rho} \right\|_F^2 \\
&+ \frac{\rho}{2} \left\| \mathbf{F}_\Omega^{k+1} - (\mathbf{Y}_\Omega - \mathbf{X}_\Omega^{k+1} - \mathcal{E}_\Omega^{k+1}) + \frac{\boldsymbol{\mu}_3^{k+1}}{\rho} \right\|_F^2.
\end{aligned} \tag{80}$$

Using the property of inequality  $(a+b)^2 \leq 2(a^2+b^2)$  with  $a, b \geq 0$ , the lower bound of each term can be estimated,

$$\begin{aligned}
&\left\| \mathbf{W}^{k+1} - \mathbf{X}^{k+1} + \frac{\boldsymbol{\mu}_1^{k+1}}{\rho} \right\|_F^2 \\
&\geq \frac{1}{2} \|\mathbf{W}^{k+1}\|_F^2 - \left\| \mathbf{X}^{k+1} - \frac{\boldsymbol{\mu}_1^{k+1}}{\rho} \right\|_F^2,
\end{aligned} \tag{81}$$

$$\begin{aligned}
&\left\| \mathbf{E}^{k+1} - \mathcal{E}_\Omega^{k+1} + \frac{\boldsymbol{\mu}_2^{k+1}}{\rho} \right\|_F^2 \\
&\geq \frac{1}{2} \|\mathbf{E}^{k+1}\|_F^2 - \left\| \mathcal{E}_\Omega^{k+1} - \frac{\boldsymbol{\mu}_2^{k+1}}{\rho} \right\|_F^2,
\end{aligned} \tag{82}$$

$$\begin{aligned}
&\left\| \mathbf{F}_\Omega^{k+1} - (\mathbf{Y}_\Omega - \mathbf{X}_\Omega^{k+1} - \mathcal{E}_\Omega^{k+1}) + \frac{\boldsymbol{\mu}_3^{k+1}}{\rho} \right\|_F^2 \\
&\geq \frac{1}{2} \|\mathbf{F}_\Omega^{k+1}\|_F^2 - \left\| \mathbf{Y}_\Omega - \mathbf{X}_\Omega^{k+1} - \mathcal{E}_\Omega^{k+1} - \frac{\boldsymbol{\mu}_3^{k+1}}{\rho} \right\|_F^2.
\end{aligned} \tag{83}$$

Furthermore, it follows from Assumption 2 that  $R(\mathbf{W}^{k+1})$  and  $\phi(\mathbf{E}^{k+1})$  are bounded. Therefore, we can conclude that the sequence  $\{\boldsymbol{\Gamma}^k\}_{k=1}^{+\infty}$  is bounded.

Thus, Theorem 10 is obtained.  $\square$

APPENDIX K  
PROOF OF THEOREM 10

*Proof.* Theorems 5-8 have demonstrated that the function  $L$  monotonically decreases and possesses a lower bound, which implies the convergence of the function  $L$ . The following conclusions can be derived from (78).

$$\begin{aligned}
\lim_{k \rightarrow +\infty} \|\mathbf{X}^{k+1} - \mathbf{X}^k\|_F^2 &= 0, & \lim_{k \rightarrow +\infty} \|\mathbf{X}_\Omega^{k+1} - \mathbf{X}_\Omega^k\|_F^2 &= 0, \\
\lim_{k \rightarrow +\infty} \|\mathbf{W}^{k+1} - \mathbf{W}^k\|_F^2 &= 0, & \lim_{k \rightarrow +\infty} \|\mathcal{E}^{k+1} - \mathcal{E}^k\|_F^2 &= 0, \\
\lim_{k \rightarrow +\infty} \|\mathcal{E}_\Omega^{k+1} - \mathcal{E}_\Omega^k\|_F^2 &= 0, & \lim_{k \rightarrow +\infty} \|\mathbf{F}_\Omega^{k+1} - \mathbf{F}_\Omega^k\|_F^2 &= 0, \\
\lim_{k \rightarrow +\infty} \|\mathbf{E}^{k+1} - \mathbf{E}^k\|_F^2 &= 0, & \lim_{k \rightarrow +\infty} \|\boldsymbol{\mu}_1^{k+1} - \boldsymbol{\mu}_1^k\|_F^2 &= 0, \\
\lim_{k \rightarrow +\infty} \|\boldsymbol{\mu}_2^{k+1} - \boldsymbol{\mu}_2^k\|_F^2 &= 0, & \lim_{k \rightarrow +\infty} \|\boldsymbol{\mu}_3^{k+1} - \boldsymbol{\mu}_3^k\|_F^2 &= 0.
\end{aligned}$$

Therefore, we can conclude that  $\lim_{k \rightarrow +\infty} \|\boldsymbol{\Gamma}^{k+1} - \boldsymbol{\Gamma}^k\|_F^2 = 0$ .

Thus, Theorem 11 is obtained.  $\square$

APPENDIX L  
PROOF OF THEOREM 11

*Proof.* Theorems 5-11 have demonstrated that the sequence  $\{\boldsymbol{\Gamma}^k\}_{k=1}^{+\infty}$  is bounded and satisfies the condition  $\lim_{k \rightarrow +\infty} \|\boldsymbol{\Gamma}^{k+1} - \boldsymbol{\Gamma}^k\|_F^2 = 0$ . According to the Bolzano-Weierstrass theorem [53], we can deduce that there must exist a subsequence  $\{\boldsymbol{\Gamma}^{k_j}\}$  of the sequence  $\{\boldsymbol{\Gamma}^k\}$ , such that  $\lim_{k \rightarrow +\infty} \boldsymbol{\Gamma}^{k_j} = \boldsymbol{\Gamma}^*$ .

Next, considering the sufficient condition for the minimization problem in Algorithm 2, which requires the following equation to be satisfied,

$$\begin{aligned}
\mathbf{W}^k - \mathbf{X}^{k+1} + \frac{\boldsymbol{\mu}_1^k}{\rho} + \mathbf{F}_\Omega^k - (\mathbf{Y}_\Omega - \mathbf{X}_\Omega^{k+1} - \mathcal{E}_\Omega^k) + \frac{\boldsymbol{\mu}_3^k}{\rho} &= 0, \\
\alpha \nabla R(\mathbf{W}^{k+1}) + \rho \left( \mathbf{W}^{k+1} - \mathbf{X}^{k+1} + \frac{\boldsymbol{\mu}_1^k}{\rho} \right) &= 0, \\
\mathbf{E}^k - \mathcal{E}^{k+1} + \frac{\boldsymbol{\mu}_2^k}{\rho} + \mathbf{F}_\Omega^k - (\mathbf{Y}_\Omega - \mathbf{X}_\Omega^{k+1} - \mathcal{E}_\Omega^k) + \frac{\boldsymbol{\mu}_3^k}{\rho} &= 0, \\
\mathbf{F}_\Omega^{k+1} + \rho \left( \mathbf{F}_\Omega^{k+1} - (\mathbf{Y}_\Omega - \mathbf{X}_\Omega^{k+1} - \mathcal{E}_\Omega^{k+1}) + \frac{\boldsymbol{\mu}_3^k}{\rho} \right) &= 0, \\
\lambda \nabla \phi(\mathbf{E}^{k+1}) + \rho \left( \mathbf{E}^{k+1} - \mathcal{E}^{k+1} + \frac{\boldsymbol{\mu}_2^k}{\rho} \right) &= 0.
\end{aligned}$$

Finally, by taking limits of the above five equations along the subsequence  $\{\boldsymbol{\Gamma}^{k_j}\}$ , we obtain

$$\begin{aligned}
\boldsymbol{\mu}_1^* &= -\alpha \nabla R(\mathbf{W}^*), & \boldsymbol{\mu}_2^* &= -\lambda \nabla \phi(\mathbf{E}^*), & \boldsymbol{\mu}_3^* &= -\mathbf{F}_\Omega^*, \\
\mathbf{W}^* &= \mathbf{X}^*, & \mathbf{E}^* &= \mathcal{E}^*, & \mathbf{F}_\Omega^* &= \mathbf{Y}_\Omega - \mathbf{X}_\Omega^* - \mathcal{E}_\Omega^*.
\end{aligned}$$

Therefore, we have demonstrated that the limit point  $\boldsymbol{\Gamma}^*$  is a stable point of formula (8).

Thus, Theorem 12 is obtained.  $\square$